12-3-2018

Lg Q of Northern, Eastern and Southeastern Alaska and Crustal Q Variations

Eric Jambo

Lg Q OF NORTHERN, EASTERN AND SOUTHEASTERN ALASKA AND CRUSTAL Q VARIATIONS

by

Eric Jambo

A Thesis

Submitted in Partial Fulfillment of the

Requirements for the Degree of

Master of Science

Major: Earth Sciences

The University of Memphis

December 2018

ACKNOWLEDGEMENTS

I would like to express my great appreciation to my thesis supervisor, Dr. Chris Cramer for his valuable support and guidance throughout this journey. His encouragement and constructive critiques kept this research project going. I would like also to express my deep gratitude to all other professors at University of Memphis especially Dr. Eric Daub and Dr. Christine A. Powell who served on my thesis committee. I thank them for valuable suggestions and inputs they gave me during the course of this project.

I also thank every student, faculty and staff member at the Center for Earthquake Research and Information (CERI) for their help during my studies. Special thanks to Arushi Saxena and Oluwaseun Idowu Fadugba for their encouragement and also to Md Nayeem Al-Noman for his contribution to this project.

And finally, I thank my late parents for their support and encouragement throughout my study and special thanks to Judy Caruthers for her generosity and life advices. I am sincerely grateful to all of them.

ABSTRACT

The increase of statewide station coverage of Alaska since 2014 due to the presence of the EarthScope USArray (TA) stations provides an unprecedented opportunity to investigate crustal attenuation in Alaska using Lg-waves. This study determines Lg-wave attenuation and its spatial variations in Alaska using 187 local and regional crustal earthquakes that occurred between June 2014 and April 2018 with M_L $\geq$4.0. An inversion is performed over ten distinct passbands 1.0 Hz, 1.3 Hz, 2.0 Hz, 3.0 Hz, 4.0 Hz, 6.0 Hz, 8.0 Hz, 10.0 Hz, 13.0 Hz, and 16.0 Hz for all waveforms with a signal-to-noise ratio greater than 2. The regression yielded the function $Q(f) = 217(\pm 28)f^{0.84(\pm 0.04)}$ $(1.0 \leq f \leq 10.0Hz)$ which represents the Alaska's frequency-dependent attenuation. Alaska displays low Q_0 and high frequency-dependence (η) which is indicative of a tectonically active region; but not as low as California or most of the Western United States..

TABLE OF CONTENTS

LIST OF FIGURES

ABBREVIATIONS

IRIS	**I**ncorporated **R**esearch **I**nstitutions for **S**eismology
RMS	**R**oot **M**ean **S**quare
SAC	**S**eismic **A**nalysis **C**ode
TA	**T**ransportable **A**rray
GMT	**G**eneric **M**apping **T**ools
AEC	**A**laska **E**arthquake **C**enter

INTRODUCTION

Background

Seismic Attenuation

In a perfectly elastic earth, seismic waves can propagate indefinitely once they are excited. But the real earth is not perfectly elastic which causes propagating waves to attenuate with time as they travel. This attenuation is due to various energy loss mechanisms.

The attenuation of seismic waves is caused by two major mechanisms: intrinsic and scattering attenuation. Intrinsic (viscoelastic) attenuation involves losing energy to heat and internal friction during the passage of an elastic wave and it is described by elastic wave theory (Shearer, 2009). The scattering attenuation, on the other hand, causes elastic energy to be scattered and redistributed into directions away from the receiver or into waves arriving in later time windows at the receiver (Cormier, 2011). It is difficult to separate the two attenuation mechanisms; therefore, in this study I will only focus on the losses due to attenuation from any mechanism.

This loss of energy causes a decrease in amplitude with time. The process of decrease in wave amplitude due to loss of energy is known as wave attenuation. The wave attenuation is represented by a dimensionless quantity Q, known as seismic quality factor, in terms of energy loss per cycle

$$\frac{1}{Q} = \frac{-\triangle E}{2\pi E} \tag{1}$$

where:

E is the peak energy and $-\triangle E$ is the energy loss per cycle (Aki and Chouet, 1975). From equation 1, the seismic quality factor Q is inversely related to the strength of attenuation. Therefore, regions with low Q value like southern California and most of western United States are more attenuating than regions with high Q value like central and eastern United States (CEUS).

Attenuation has been observed to be mostly frequency-independent in the frequency range about 0.001 to 0.1 Hz (Stein and Wysession, 2003). However, numerous studies like McNamara (2000), Erickson et al. (2004), and Benz et al. (1997) among others, have reported a dependence at higher frequencies. This frequency dependence is commonly modeled using the power law of the form

$$Q(f) = Q_0(\frac{f}{f_0})^{\eta} \tag{2}$$

where:

f_0 is a reference frequency (generally 1 Hz)

Q_0 is Q at the reference frequency, and

η is assumed to be constant over the frequencies of interest (Benz et al., 1997).

Understanding seismic attenuation is essential in earthquake hazard studies and determining crustal variations and interpreting seismic velocity anomalies associated with these variations. How rapidly the attenuation occurs, and how it depends on frequency of the seismic waves is important for defining velocity models of the crust and interpreting lateral variations of velocity and attenuation in terms of temperature and composition of the earth (Chiu and

Snyder, 2014). In addition, the decay with distance of ground motion inputs is crucial in the design of earthquake resistant structures and earthquake hazard forecasting because uncertainties in ground motion attenuation cause uncertainties in probabilistic hazard analysis (Main et al., 2011).

Lg waves

The Lg phase can be modeled as high frequency (0.2-5 Hz) crustal-guided surface waves (Knopoff et al., 1973). Lg waveforms provide a good measure of apparent crustal attenuation because they propagate as multiply reflected shear waves trapped within the crust (Bouchon, 1982). Lg is often the strongest phase on the seismogram at regional distances from 2° to 25° with average group velocity of 3.5 km/s (Aki, 1969). The figure below illustrates Lg waveforms at different stations in Alaska for an earthquake that occurred at 8.9 km depth.

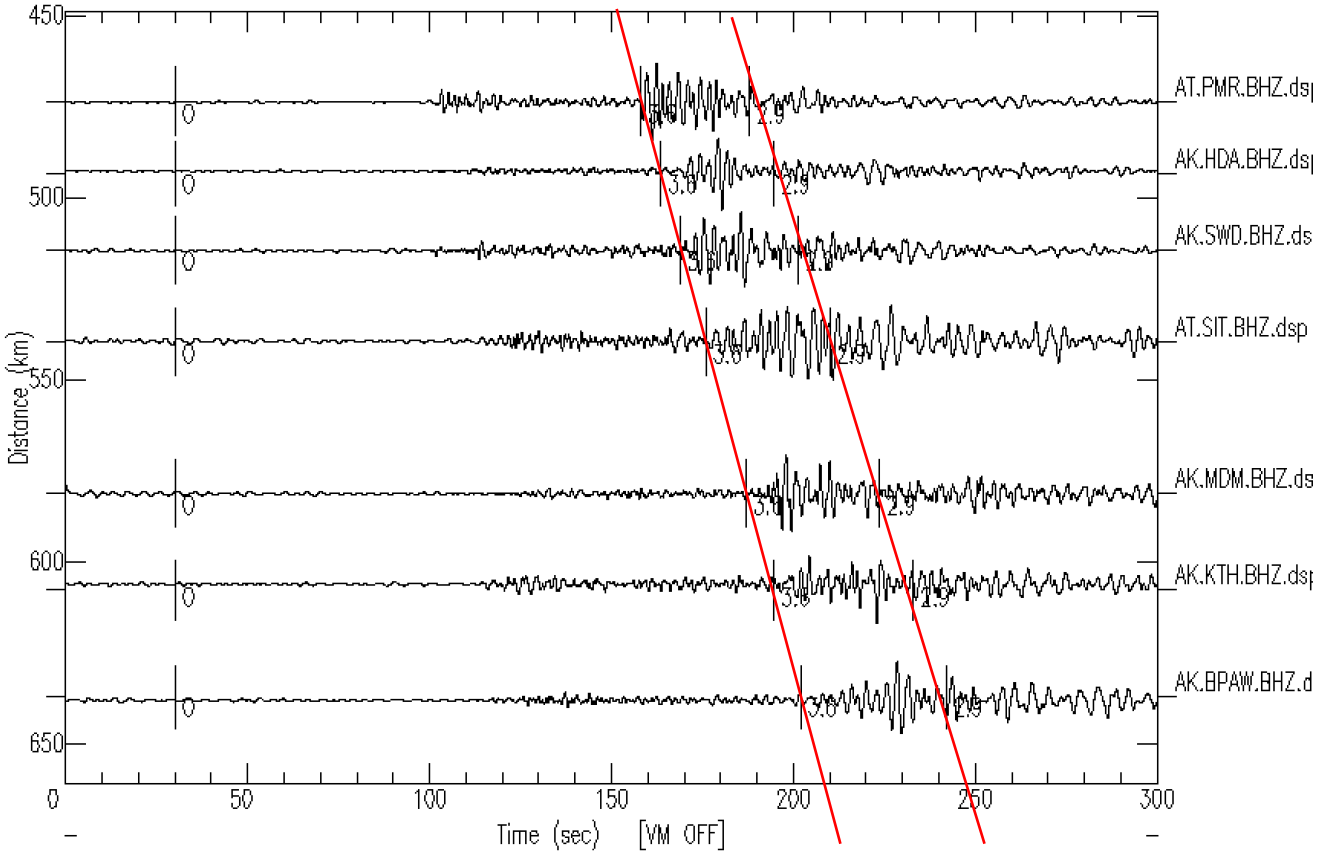

FIGURE 1: Vertical displacement seismograms from an earthquake on June 05^{th}, 2014 in southeast Alaska. The expected Lg window is bracketed by red lines on the seismograms.

Due to its sensitivity to structural variations and heterogeneities, the Lg wave is used in studying regional attenuation within the crust [Hansen et al. (1998), Benz et al. (1997), Phillips and Stead (2008) among others], magnitude estimation of shallow events [Nuttli (1973), Herrmann and Nuttli (1982)], discriminating manmade sources like explosions from natural earthquakes (Kim and Richards, 2007), and mapping crustal heterogeneities (Kennett, 1986). However all these studies are done for continental crust because the Lg phase cannot propagate in the oceanic crust due to its thin structure (Kennett, 1986); therefore, it can be used to detect the boundary between ocean and continental crust as well [Mousavi et al. (2014) and Furumura et al. (2014)]. From all these numerous studies,

it is suggested that Lg wave attenuation is strongly correlated to the age of the crust, variations in crustal thickness, crustal deformations, and thermal status of the crust.

Lg wave propagation is sensitive to lateral crustal variations. This correlation between Lg waves and crustal heterogeneity has been demonstrated in numerous studies that have been conducted around the world. In the Tibetan plateau for example, Xie (2002), McNamara et al. (1996), and Fan and Lay (2003) concluded that the high attenuation of Lg waves within the plateau was due to scattering along fractures and faults bounding the tectonic terranes that make up the plateau. Furthermore, this high attenuation is attributed to the presence of crustal deformation, tectonic activity, and interstitial fluids within the plateau. Another study by Mousavi et al. (2014) observed the presence of an Lg blockage zone in the continental margin of Nova Scotia after analyzing the attenuation of Lg waves in eastern Canada.

The relation between the Lg phase and crustal variations can be used to distinguish between tectonically active and stable regions. In stable continental regions like North Africa, Lg can be observed at a distance as great as 6000 km (McNamara, 2000). On the other hand, in tectonically active regions like California, it cannot be observed at a distance greater than 500 km (Erickson et al., 2004).

Different phases including Sn and Pn have been used to study seismic attenuation [Chiu and Snyder (2014) and Mousavi et al. (2014)]. However the Lg phase is the best candidate to use in this study not only because it is widely used in crustal attenuation Q studies [Xie (2002), Phillips and Stead (2008), Erickson et al. (2004), Mousavi et al. (2014), and McNamara (2000) among others], but also for its small-energy leakage into the mantle

(Bath, 1954) and its sensitivity to crustal structure, composition, and temperature in the waveguide along its path (Kennett, 1986).

Motivation

EarthScope USArray (TA) Project

Alaska is a seismically active state. Its seismicity varies in magnitude and spreads across the entire state including regions that have never been closely monitored (see figures 2 and 4). These earthquakes can be deadly and very damaging like the 1964 Great Alaska earthquake of magnitude 9.2 that claimed 139 lives and the damage was estimated at more than 300 millions US dollars. In 2014 the EarthScope USArray (TA) project started installing 191 new stations (155 in Alaska and 36 across northwestern Canada) that will run through 2019. New USArray TA stations were installed outside the footprint of the existing regional network. By the end of the 2017 field season, the installation was finished and the array was a grid of 280 TA stations spaced about 85 km apart covering all of mainland Alaska and parts of the Yukon, British Columbia, and the Northwest territories (Figure 3).

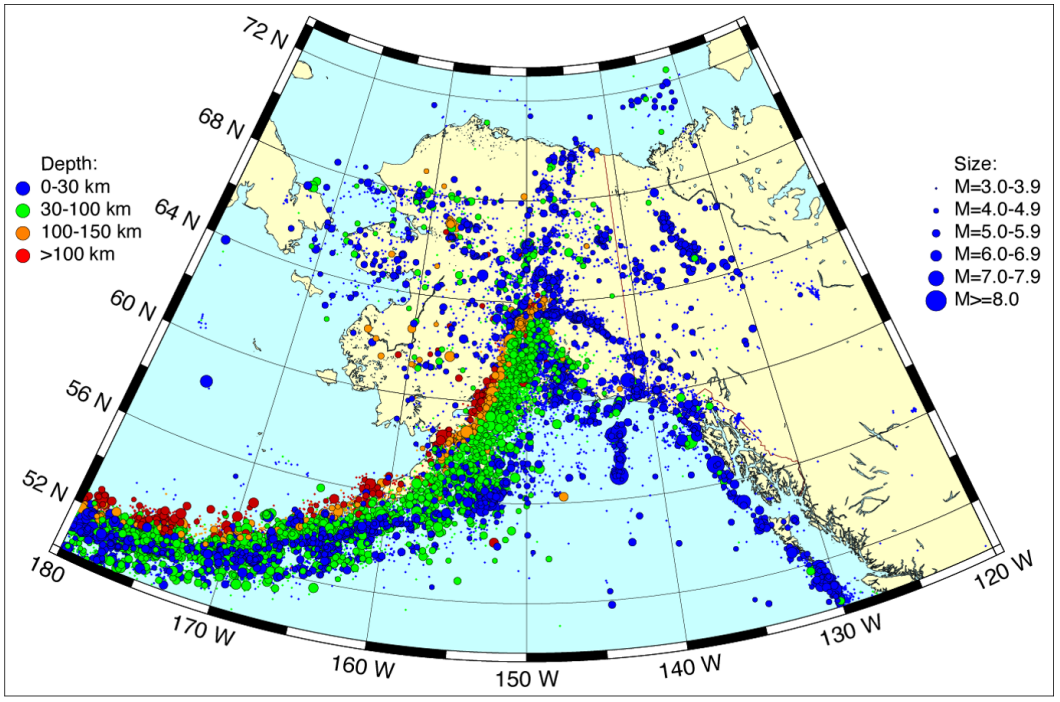

FIGURE 2: Seismicity from 1970-2012 for Alaska and vicinity from the Alaska Earthquake Center and USGS PDE catalogs. Figure taken from USArray website (www.usarray.org/alaska).

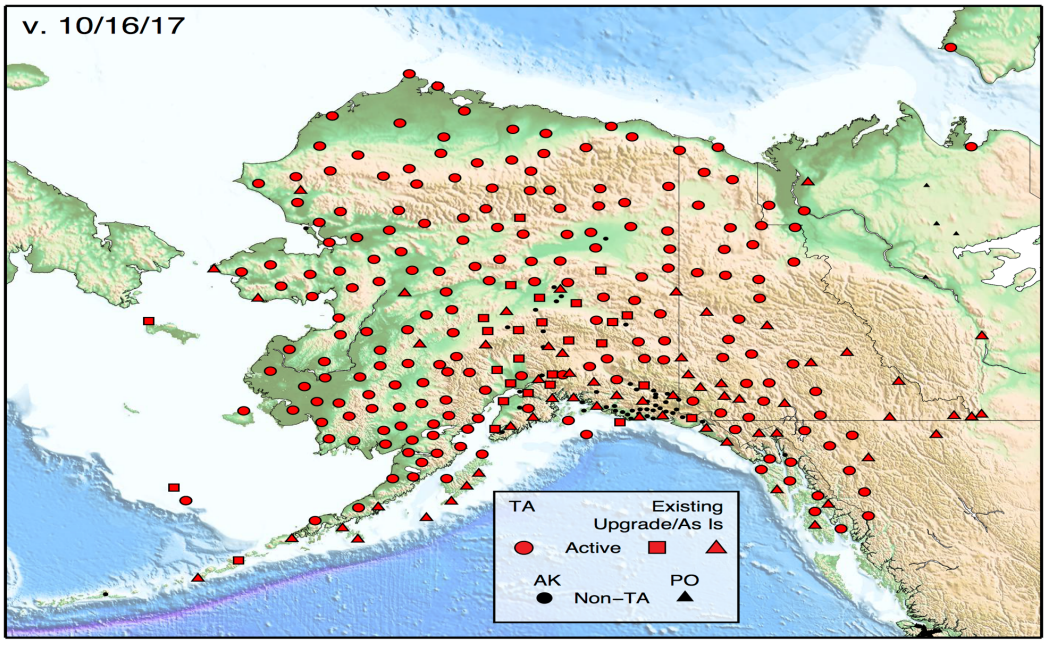

FIGURE 3: Current TA Footprint in red. ●.are new TA seismic stations. "Existing" sites are either upgraded (■.) or as-is (▲.) Collaborating networks in black (Alaska Earthquake Center, Alaska Volcano Observatory, Alaska Tsunami Warning Center, Yukon Northwestern Seismic Network). Figure taken from USArray website (www.usarray.org/alaska).

There were two previous studies of seismic attenuation in Alaska [(Hansen et al., 1998), (McNamara, 2000), and (Stachnik et al., 2004)]. These studies focused in south-central Alaska due to limited data available during the course of these studies. Before the EarthScope USArray TA project in Alaska, most existing seismic stations were concentrated near highways and close to the subduction zone (Figure 4). With the addition of TA stations in previously unmonitored areas of Alaska, there is an opportunity to improve our estimates of location and size of earthquakes. The improvement in our ability to detect smaller earthquakes in the region, especially in the northern and western portions of the state, where previously there have been very few stations deployed (see Figure 4), will enable a better understanding of active faults that can generate larger and damaging earthquakes and will help to characterize seismic hazards related to these faults.

Furthermore, this unprecedented statewide station coverage presents an opportunity to understand crustal attenuation and the structure of the earth beneath Alaska and hopefully improve the results in areas like south-central Alaska that have been studied before by incorporating a relatively large data set of observations. By estimating the attenuation relationships, we will provide input parameters such as the frequency-dependent quality factor function $Q(f)$ necessary to develop better Ground Motion Prediction Equations (GMPEs). GMPEs are efficiently used to estimate ground motions in both deterministic and probabilistic seismic hazard analyses. Not only will this support the development of seismic hazard products, the same information will improve the reliability of ShakeMaps which are used in planning and response exercises for large earthquakes.

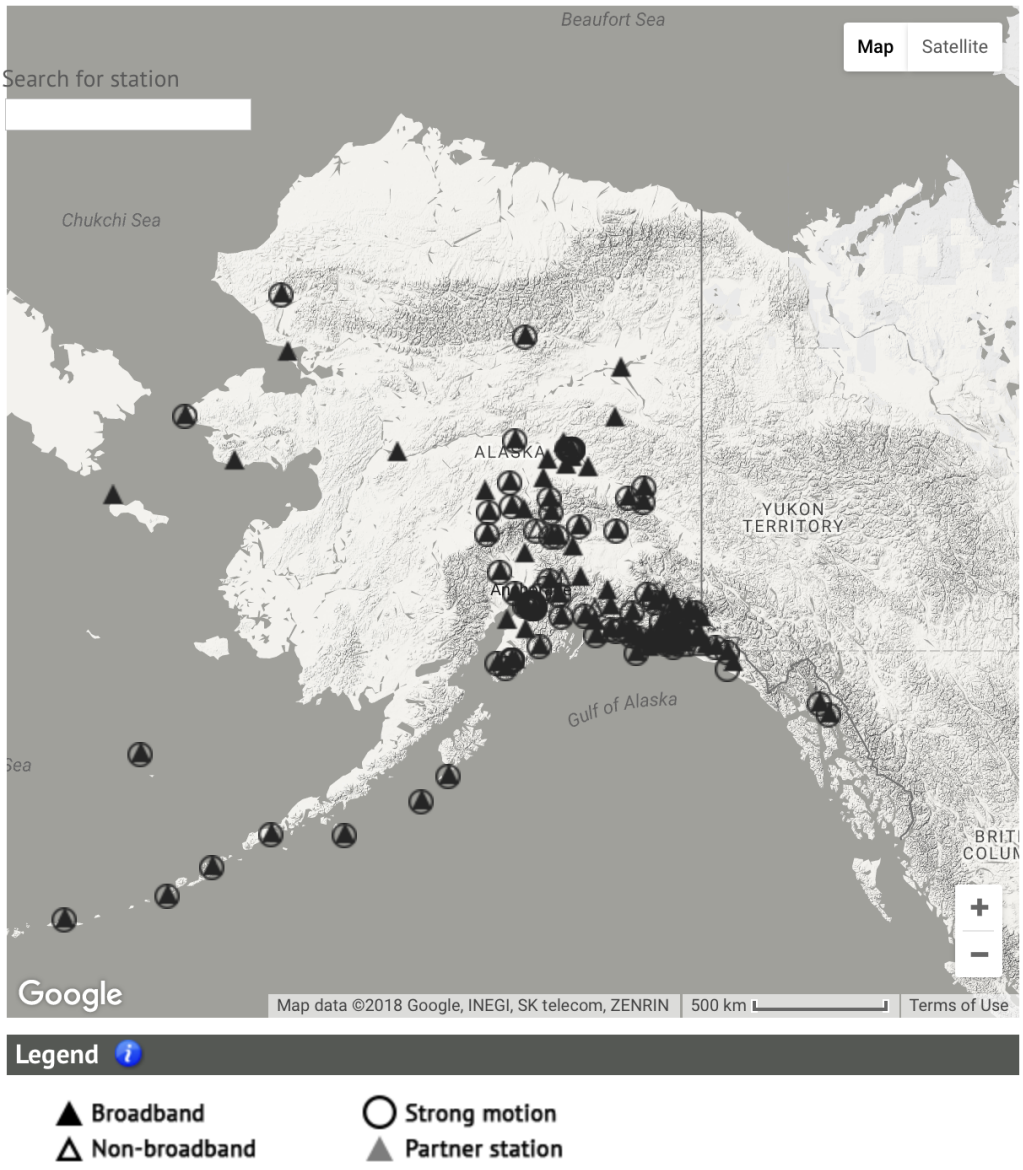

FIGURE 4: Alaska Network stations before EarthScope USArray (TA) project. Figure taken from AEC website (www.earthquake.alaska.edu/network).

LITERATURE REVIEW

Previous Studies

In a previous study using Lg waves to determine the Q attenuation in south-central Alaska, the frequency-dependent quality factor in this region is given by the equation $Q(f) = 220(\pm 30)f^{0.66(\pm 0.09)}$ $(0.75 \leq f \leq 12.0Hz)$ (McNamara, 2000). The Q_0 and η values determined from McNamara (2000) indicate a tectonically active region with high crustal attenuation. Similar results were obtained in the Caribbean where $Q(f) = 235f^{0.65}$ $(0.1 \leq f \leq 12.8Hz)$ (Hosseini et al., 2015) and Basin and Range province in the western United States where $Q(f) = 200(\pm 40)f^{0.68(\pm 0.16)}$ $(0.75 \leq f \leq 12Hz)$ (Erickson et al., 2004). These regions stated above are less attenuating than northern and southern California where $Q(f) = 152(\pm 37)f^{0.72(\pm 0.16)}$ $(0.75 \leq f \leq 7.0Hz)$ and $Q(f) = 105 \pm 26)f^{0.67(\pm 0.16)}$ $(0.75 \leq f \leq 7.0Hz)$, respectively (Erickson et al., 2004). In addition, the η value from McNamara (2000) suggests that both scattering and intrinsic attenuation mechanisms likely play an equal role in attenuating Lg energy in south-central Alaska. This is supported by the results obtained using S-wave coda decay (Steensma and Biswas, 1988).

Tectonic History and Geology of the region

Alaska is located at the northern end of the active plate boundary between the Pacific plate and the North American plate. The Pacific plate subducts in a northwestern direction at a rate of 54 mm/year beneath south-central Alaska (Brocher et al., 1994).

This northwestern movement of the Pacific plate exerts a massive amount of force on Alaska and yields large earthquakes, deforms the crust, and generates volcanoes in the Aleutian trench and the mainland Alaska. Plate boundary deformation associated with subduction along the Aleutian-Alaska subduction zone affects crustal Alaska all the way to the North in the Brooks Range. In addition to the subduction motion that drives Alaska's tectonics and seismicity, the transform motion in the southeast Alaska also builds stress along the Pacific and North American plate boundaries and generates numerous shallow earthquakes and faults in this area.

Numerous fault systems and high mountain ranges present across Alaska accomodate the compressing of the land in the north-south direction and shearing of southern Alaska towards the West. These mountain ranges include the Brooks Range in the North, the Alaska Range in central Alaska and the Aleutian Range in the southwest. The faults in Alaska include active and inactive faults. Active faults include the Fairweather-Queen Charlotte strike-slip fault in the south, the McGinnis Glacier fault and the Totschunda fault which belong to the Denali fault system in the Alaska Range, and Tintina fault and Kaltag fault in the sourrounding areas of the Alaska Range (Brogan et al., 1975). Figure 5 shows the locations of some of the faults mentioned above and many others present in Alaska.

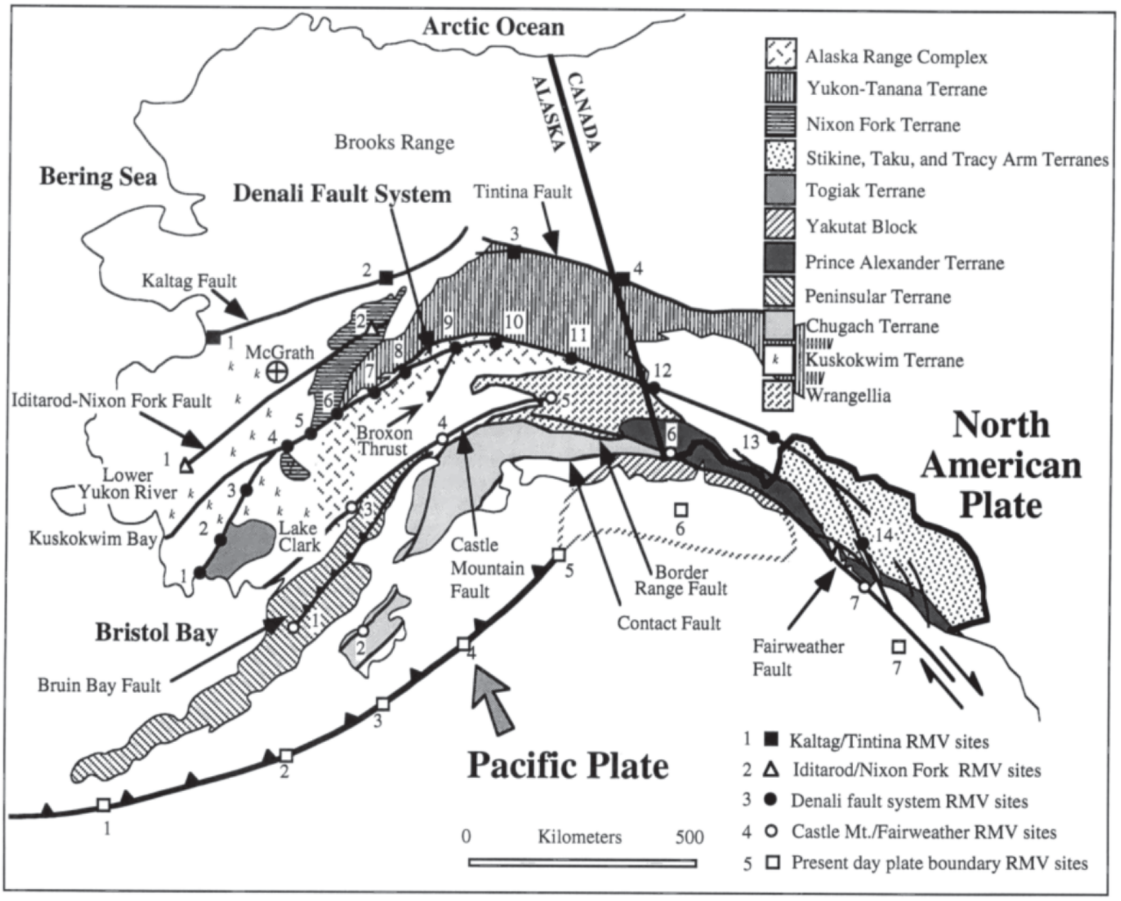

FIGURE 5: Faults and Terranes in Alaska. Redfield and Fitzgerald (1993).

Major fault systems are located on the boundaries of the structurally bound lithotectonic terranes and sub-terranes resulted from hundreds of million years of tectonic evolution in Alaska (Plafker and Berg, 1994). The Alaska terranes are in a complex pattern reflecting interactions of the oceanic plates with the North American plate which result in translation and rotation movements of the two plates. Furthermore, they include dispersed rotated noncrystalline and crystalline fragments of North American continental crust (Plafker and Berg, 1994).

These terranes are grouped into composite terranes (CTs) based on similarity in their lithotectonic settings and tectonic evolution. These composite terranes include the Arctic

CT, Central CT, Yukon CT, Togiak-Koyukuk CT, Oceanic CT, Wrangellia CT, and Southern Margin CT (Figure 6) (Plafker and Berg, 1994). These composite terranes have been forming over millions of years that are divided in 8 different periods that followed the Precambrian era. The 8 evolution periods that followed the Precambrian and the tectonic activities that occurred in each period, as discussed by Plafker and Berg (1994), are summarized in table 1.

In past studies, it has been shown that Q values depend on the type of rocks found in the study region and their age (Mitchell and Hwang, 1987). Regions characterized by hard, competent rocks usually have high Q values while areas characterized by soft, molten rocks such as volcanic areas usually have low Q values (Phillips and Stead, 2008). In other studies, tectonic structures like faults and ocean basins were found to affect Lg wave propagation because of its sensitivity to the structural variations and heterogeneities [(McNamara, 2000) and (Erickson et al., 2004)]. Therefore, understanding the tectonic history and geology of the study area can lead to a better understanding and interpretation of its attenuation results.

Table 1: Summary of Tectonic Activity in Alaska.

Timeline	**Tectonic Activity**
Cambrian to Late Devonian (570-360 Ma)	-Continued subsidence and local rifting along the passive margine of the continent. -Deposition of carbonate rocks and clastic sediments. -Local extension and Bimodal volcanism in parts of the Central and Yukon CTs. -Early Paleozoic subduction and arc volcanism along the Arctic CT. -Silurian deformation of the inboard part of the Arctic CT. -Compressional and elastic deformations.
Early Mississippian to Middle Triassic (360-230 Ma)	-Deposition of continental clastic rocks, carbonate rocks, and chert on subsiding ocean-facing shelf. -Rise of the Arctic CT.
Late Triassic to Late Jurassic (230-160 Ma)	Convergence between Farallon plate and the continental margin.
Late Jurassic to Aptian (160-120 Ma)	Convergence followed by arc magmatism, accretion, and deformation along western continental margin.
Aptian to Campanian (120-84 Ma)	-Orthogonal to dextral oblique convergence on the boundary of the Farallon and North American plates. -Deformation and rotations of the Canada basin.
Campanian to Paleocene (84-66 Ma)	Terranes along the Northeast Pacific ocean margin took their current configuration.
Paleocene to Mid Eocene (66-50 Ma)	Continuation of large Kula-North American plate relative motions in Alaska and adjacent parts of Canada.
Eocene to Present(50-0 Ma)	-Subduction of then Kula plate. -Beginning of the current north to northwest motion of the Pacific plate relative to continental margins of Alaska and most of Canada.

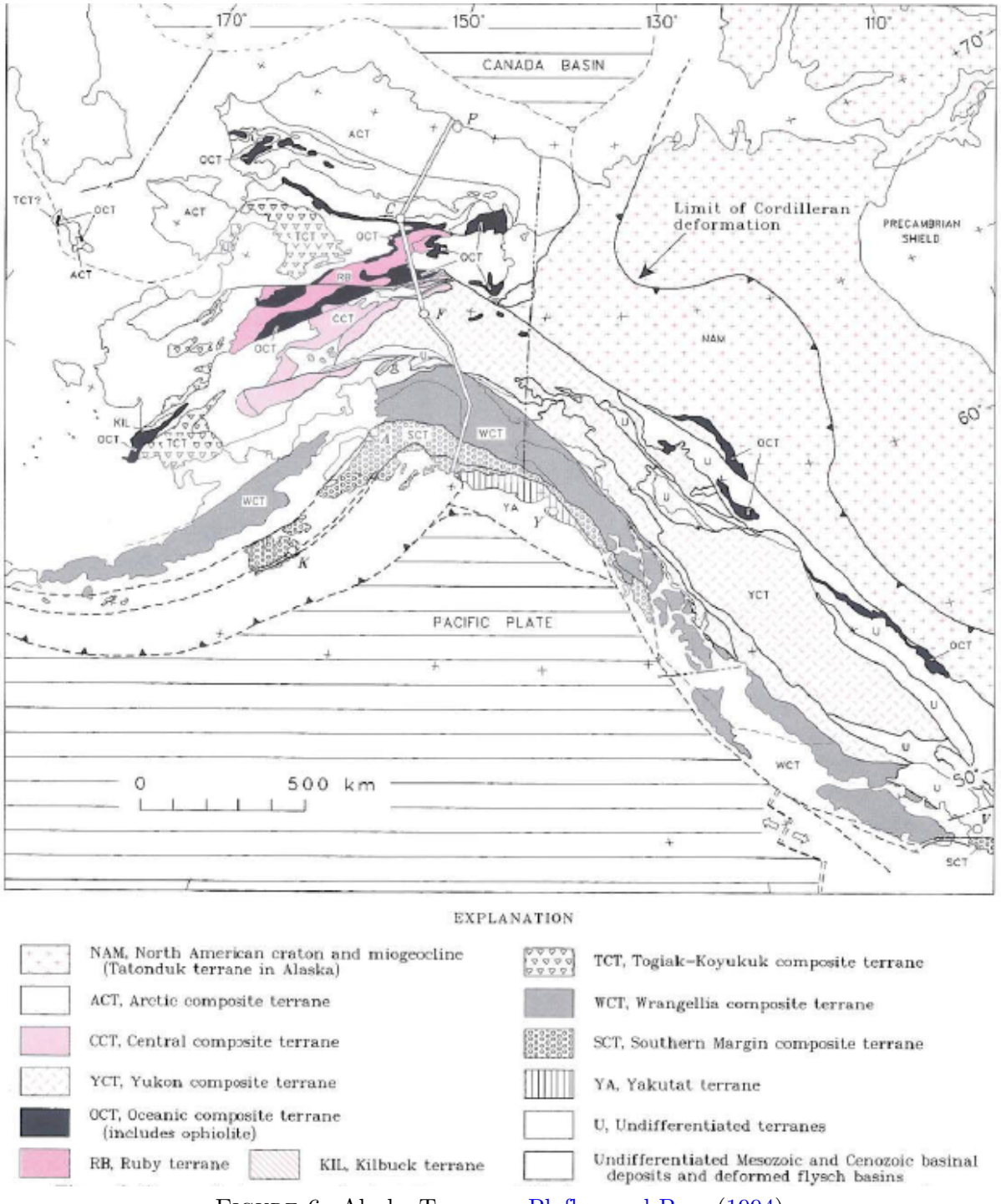

FIGURE 6: Alaska Terranes. Plafker and Berg (1994).

DATA ANALYSIS AND METHODOLOGY

Background Theory

During an earthquake, the source amplitude is affected by the condition of the rocks it travels through also known as the path effect, the geology of the site at which the recording station is located, and the recording instrument gain. Therefore, the seismic signal observed at any seismogram is a combination of the source function which represents the source that emitted the seismic wave, the path effect which is modeled by a combination of geometrical spreading and anelastic attenuation functions, the site amplification factor because the site geology may amplify or deamplify the amplitude, and the instrument gain factor. The observed Lg spectral amplitude A of an earthquake at a given hypocentral distance r in function of frequency f can be written as

$$A_{Lg}(r, f) = R_{\theta,\phi} S(f) I(f) G(f) r^{-\gamma} e^{\frac{-\pi f r}{Q\beta}} \tag{2.3}$$

where $R_{\theta,\phi}$ is the radiation pattern factor, $S(f)$ is the source spectrum, $I(f)$ is the instrument response, $G(f)$ is the site amplification, γ is the geometrical spreading factor (usually 0.5), β is the average group velocity of the phase (assumed to be 3.5 km/s) and Q is apparent attenuation. Intrinsic and scattering attenuation are both combined in this parameter Q.

Using equation 2.3 when the radiation pattern is assumed to be averaged out over multiple events and paths, the expected instrument corrected spectral amplitude, A, of Lg at frequency f for the j^{th} earthquake recorded at the i^{th} station can be modeled as

$$A_{ij}(f) = r_{ij}^{-\gamma} S_j(f) G_i(f) e^{\frac{-\pi f r_{ij}}{Q\beta}} \tag{2.4}$$

Using an inversion method, we can solve for any of the terms in equation 2.4 including apparent attenuation Q for any given area as we did in this study for Alaska.

Tok Earthquake Analysis

Data Selection

In this study, we initially processed horizontal seismograms recorded from the Tok earthquake. The Tok earthquake occurred on February 13^{th}, 2017. It had a magnitude of 5.3 M_L and focal depth of 8.9 km. By specifying four different azimuth ranges, we defined four profiles of interest in the area surrounding the earthquake epicenter in central Alaska. These profiles were the southwestern profile (-180° to -90°), the northwestern profile (-45° to -15°), the northeastern profile (15° to 45°), and the southeastern profile (120° to 165°) (Figure 7 - 10). We used data recorded at stations located within 20° (2200 km) of the epicenter to study the frequency-dependence of Lg wave attenuation and the crustal Q variations in each profile. The figures below represent the defined profiles.

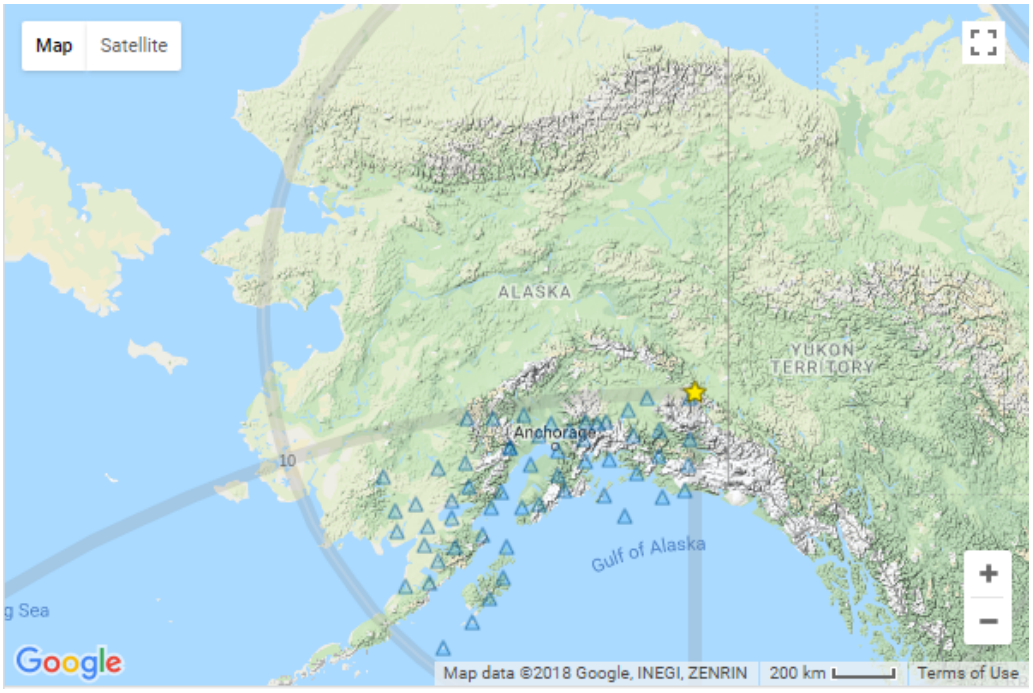

FIGURE 7: Southwestern profile (-180° to -90°).
The yellow ★ is the epicenter of Tok earthquake. △. represents every operational station during this event. Figure obtained from IRIS website (http://ds.iris.edu/wilber3/find_event).

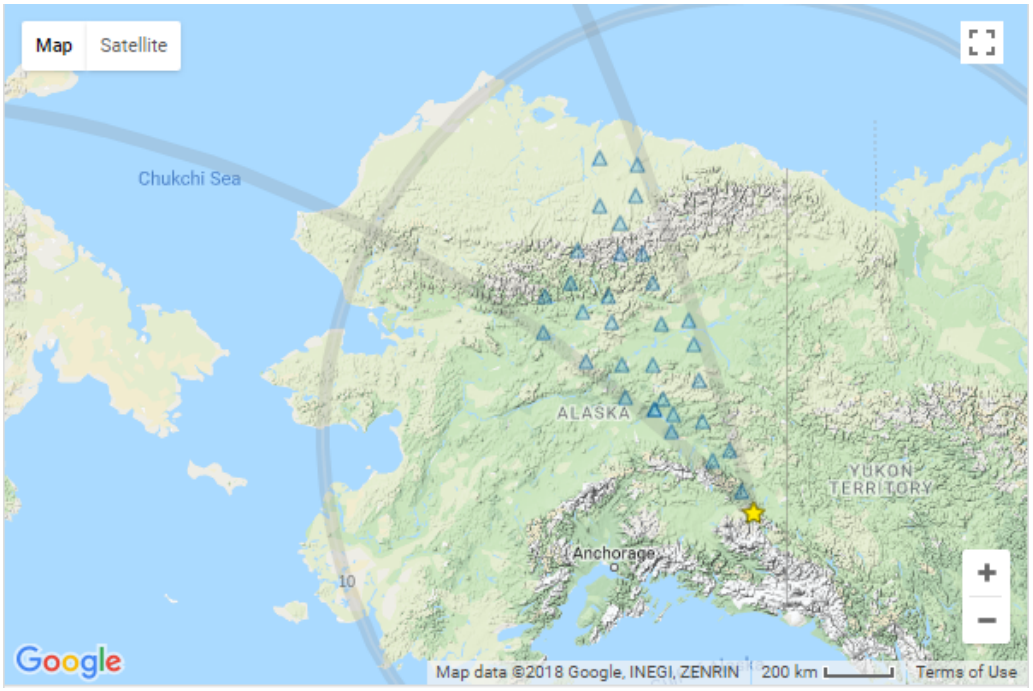

FIGURE 8: Northwestern profile (-45° to -15°).
Symbols and source are the same as in Figure 7.

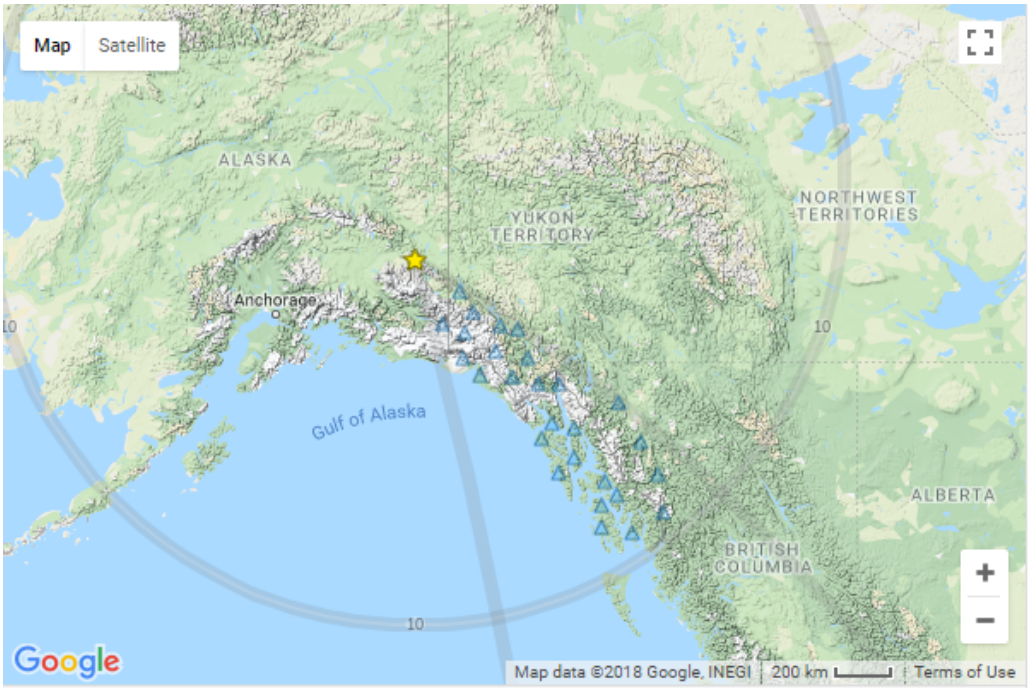

FIGURE 9: Southeastern profile (120° to 165°).
Symbols and source are the same as in Figure 7.

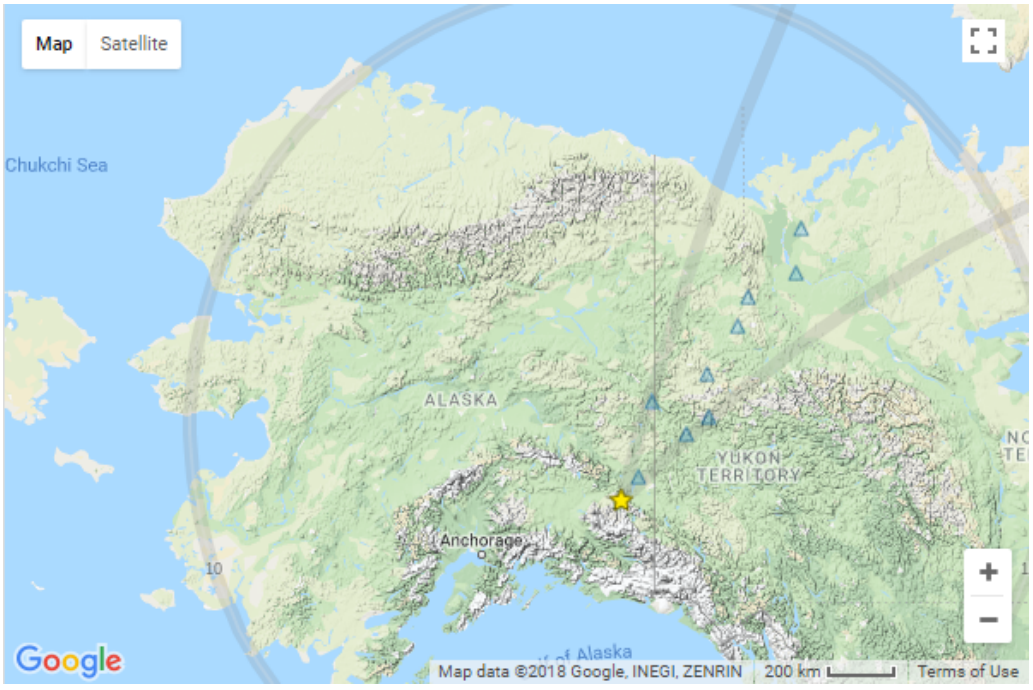

FIGURE 10: Northeastern profile (15° to 45°).
Symbols and source are the same as in Figure 7.

Data Processing

The pre-processing step consisted of three similar procedures for all the defined profiles. The first was downloading data recorded on all three components from archives curated by the IRIS Data Management Center for each of the profiles. The second was picking p-wave arrival times to indicate the end of pre-event noise. And the last was removing the instrument response from the observed measurements.

After the instrument correction, we measured the amplitude of the velocity waveform in the frequency domain using the fast Fourier transform. Then we picked the filter corners by marking the start and end of the velocity signal in each waveform to bracket in all the characteristic frequencies of the S-Lg spectra and filtered the velocity records.

After velocity record filtering, we applied a series of bandpass filters with ten center frequencies (f) to the obtained waveforms and extracted frequency-dependent amplitude estimates at each station. For these estimates we used both horizontal components. This approach is similar to the one described in McNamara et al. (1996), Benz et al. (1997), and Erickson et al. (2004). The only difference is the use of velocity records instead of tangential displacement in the analysis. The bandpass center frequencies used are 1.0, 1.3, 2.0, 3.0, 4.0, 6.0, 8.0, 10.0, 13.0, and 16.0 Hz. For each passband, the lower limit is set at $0.025log_{10}(f)$ below the center frequency f and the upper limit is set at $0.025log_{10}(f)$ above the center frequency f.

With the amplitude estimates at each center frequency f, we fit them into a linear equation of the form

$$ln(y) = A + Cr_0 - \gamma ln(r_0) \tag{2.5}$$

where r_0 represents the epicentral distance, y represents the amplitude estimate at frequency f, γ is the geometrical spreading exponent, and A and C are constants used to get Q estimates (Cramer, 2018).

Notice that equation 2.5 is similar to equation 2.4 after taking natural logarithm of both sides of equation 2.4 and rearranging the terms in the case of one event. Therefore, the constant $A = lnS(f) + lnG(f)$ and the constant $C = \frac{-\pi f}{Q\beta}$. The epicentral distance ranges between 100 - 2000 km and the average shear wave velocity (β) and γ were assumed to be 3.5 km/s and 0.5, respectively. We get Q estimates by inverting for C and then solving equation $C = \frac{-\pi f}{Q\beta}$ for Q at each frequency f. After obtaining the Q estimates, we determined the frequency-dependent Q function of each profile by fitting all Q estimates at all frequencies into the equation 2.

In order to fit $Q(f) = Q_0(\frac{f}{f_0})^\eta$ to the obtained Q estimates, we use a linear least-squares regression analysis based on the elimination method as it was done by Cramer (2018).

Taking the logarithm of both sides of equation 2 yields:

$$lnQ(f) = lnQ_0 + \eta ln(f) \tag{2.6}$$

where lnQ_0 and η are the unknowns to be determined when the reference frequency f_0 is set equal to 1.0 Hz. The result is a linear equation of the form $Q(f) = Q_0 f^\eta$ representing the frequency-dependency attenuation in each profile.

2014-2018 events Analysis

Data Selection and Preparation

The seismic data used in this study were obtained from 187 local and regional crustal earthquakes that occurred and were recorded at various sites within Alaska and Western Canada from June 1^{st}, 2014 to April 15^{th}, 2018. The data recordings were requested from archives curated by the IRIS Data Management Center. Figure 11 shows the locations of all events and the corresponding recording stations. Alaska is known for a large number of small and moderated-sized earthquakes; however, the events used in this study were limited to earthquakes with magnitude greater than 4.0 in order to have a good signal to noise ratio over large distances. These earthquakes must have happened at focal depths less than 30 km to account for crustal events only. In addition, the events were limited to the ones that were recorded by at least 3 stations in order to reduce the trade-off between source and receiver terms in the inversion.

Furthermore, the events were limited in a range of epicentral distance of 100 to 1000 km to use good quality data. At epicentral distances less than 100 km the faster crustal and upper mantle waves like S waves are still mixed with the Lg waves; therefore, we omitted the records with epicentral distances less than 100 km to distinguish the Lg phase from other regional phases. Furthermore, we omitted the records with epicentral distance greater than 1000 km because the earthquake signal gets lost in the background noise. All the seismic waveforms used in this part of the study were recorded on vertical

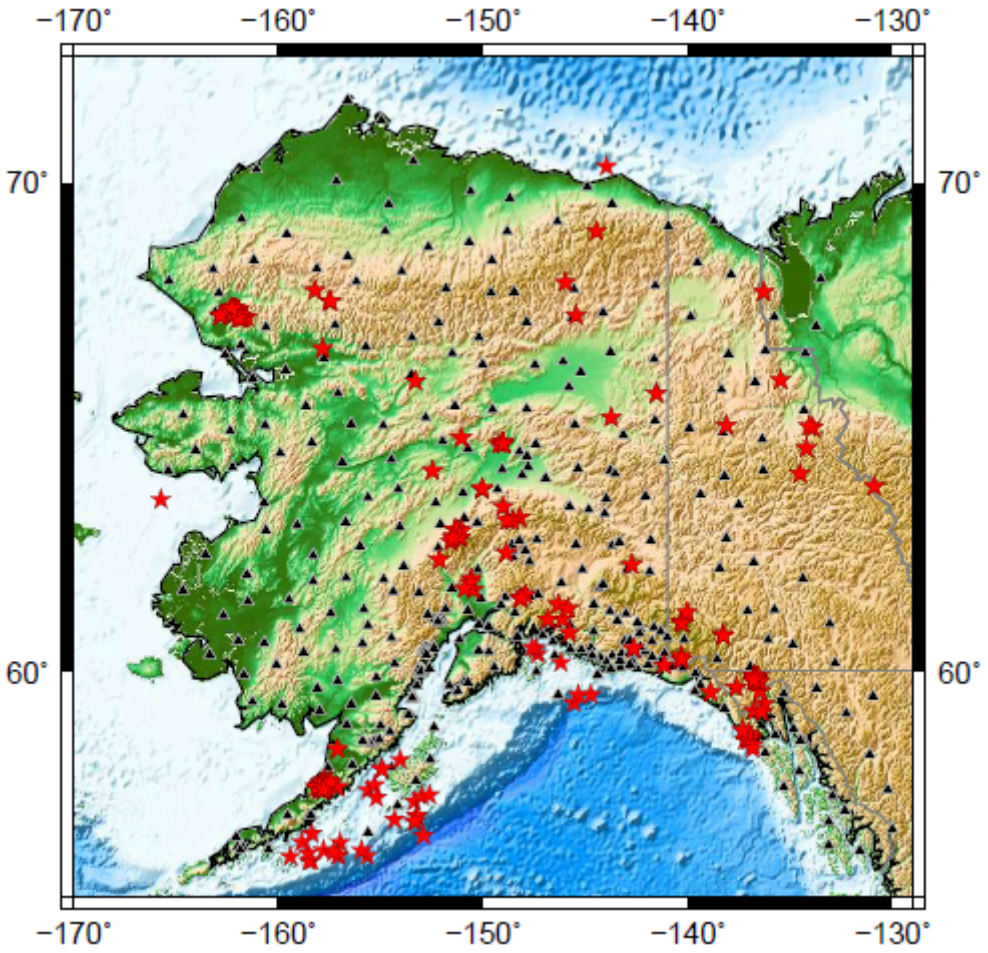

FIGURE 11: Seismicity data used in this study. Red ★ are earthquakes and ▲ are recording stations. The figure was generated using GMT. An open source software available at: http://gmt.soest.hawaaii.edu.

(Z) component and downloaded 30 s prior to and 600 s after the origin time of every event.

We inspected all downloaded data (366 events) to remove the offshore events except the ones located in the Alaska crustal wedge above the subduction zone and a few others of particular interest. Although this process reduced the number of events to be used in half (Figure 11), we were left with a set of 187 events for our analysis. Then we converted the reported magnitudes to moment magnitude as it is the widely used magnitude scale in seismic attenuation. Because there were only a few events reported in moment magnitude,

where possible we used the moment magnitudes obtained from the St. Louis regional moment tensor website (http://www.eas.slu.edu/eqc/eqc_mt/MECH.NA/) as substitutes for the events reported in other magnitudes scales. For the remainder of the events their moment magnitudes values were estimated using the magnitude conversion models for Alaska and western Canada (Ruppert and Hansen, 2010).

Data Processing

The pre-processing steps consist of seismic phase windowing, data quality analysis, and instrument correction. We defined seismic phases in time windows using their known velocity ranges in order to facilitate recognition of the Lg phase. The first arriving body waves Pn and P-coda were windowed using the velocity ranges of 7.8 - 8.1 km/s and 5.8 - 4.8 km/s, respectively while the Lg wave was windowed in the range of 3.6 - 2.9 km/s. After defining different phases in time windows, we removed all waveforms recorded at stations with recording issues and bad quality data. Finally we corrected the amplitude by removing the instrument response from the seismograms using Seismic Analysis Code (SAC) (Goldstein et al., 2003).

After obtaining the velocity records, we filtered them in ten frequency passbands with center frequencies f set at 1.0, 1.3, 2.0, 3.0, 4.0, 6.0, 8.0, 10.0, 13.0 and 16.0 Hz for all stations. A similar approach is used in many Lg attenuation analyses and is described in McNamara et al. (1996), Benz et al. (1997), and Erickson et al. (2004). The only difference is the use of velocity records instead of tangential displacement in this analysis. For each station, the filtering was constrained to frequency bands with center frequencies below half of the Nyquist frequency. Consequently, the analysis in this study was done

only in eight frequency bands centered at 1.0, 1.3, 2.0, 3.0, 4.0, 6.0, 8.0, 10.0 Hz. For each passband with center frequency f, the lower limit is set at $0.025log_{10}(f)$ below f and the upper limit is set at $0.025log_{10}(f)$ above f.

In order to obtain high quality Lg amplitude measurements for Q estimation, we did a two-step signal to noise quality analysis. We measured the root-mean square (RMS) amplitude for both Lg and P-coda phases, then we calculated the signal-to-noise ratio (SNR) using the Lg phase as signal and the P-coda as noise. The noise window with the same length as the Lg window used in this study is picked from a time window which immediately preceeds the Lg window.

The final step of data processing was obtaining Lg spectral amplitude at every frequency of interest. This process was only performed on stations with signal to noise ratio greater than two (SNR $\geq$ 2). For the stations that passed this signal to noise ratio constraint, the Lg phase peak amplitude is reported as the amplitude associated with the center frequency f of the frequency passband of interest.

Q Inversion

The inversion method used in this study to estimate the frequency dependence of Lg attenuation has been detailed and successfully applied in the continental United States by Benz et al. (1997) and Erickson et al. (2004), and further implemented in the continental margin of Nova Scotia by Mousavi et al. (2014), in south-central Alaska (McNamara, 2000), Tibetan plateau (McNamara et al., 1996), and in the Caribbean region (Hosseini et al., 2015).

Following the approach of McNamara et al. (1996), we take the logarithm of both sides of equation 2.4 and rearrange the terms considering a known geometrical spreading exponent. It yields:

$$ln[A_{ij}(f)] + \gamma ln r_{ij} = lnS_j(f) + lnG_i(f) - \frac{\pi f r_{ij}}{Q\beta} \tag{2.7}$$

in which the left-hand side consists of known parameters and the right-hand side consists of unknown arguments.

When the corrected amplitude for the geometrical spreading is plotted against epicentral distance, the right-hand side of equation 2.7 represents a straight line whose intercept is controlled by the source and receiver terms and its the slope is controlled by $Q^{-1}(f)$. Therefore, based on equation 2.7, a system of linear equations can be set up using event-station pairs in the linear inversion problem

$$\mathbf{Gm} = \mathbf{d} \tag{2.8}$$

where $\mathbf{G}$ is the kernel matrix made up of the parameter coefficients of equation 2.7. It consists of mostly ones and zeros, and a portion of one column listing the last term of equation 2.7. The vector $\mathbf{m}$ is the unknown vector to be determined and is composed of $S_j(f)$, $G_i(f)$, and $Q^{-1}(f)$. The $\mathbf{d}$ vector is comprised of the left-hand side of equation 2.7.

Equation 2.8 has $ij + 1$ unknowns for ij number of equations; therefore, we use an additional constraint for the receiver terms by requiring that the sum of all the station

terms equals zero (Ottemöller et al., 2002):

$$\sum_i ln[G_i(f)] = 0. \tag{2.9}$$

Based on equation 2.7 and the constraint in equation 2.9, the matrices in equation 2.8 can be written as follows:

$$\begin{bmatrix} 1 & 0 & \dots & 0 & 1 & 0 & 0 & \dots & 0 & 0 & \frac{-\pi f r_{11}}{\beta} \\ 1 & 0 & \dots & 0 & 0 & 1 & 0 & \dots & 0 & 0 & \frac{-\pi f r_{12}}{\beta} \\ \vdots & \vdots & \vdots & \vdots & \vdots & \vdots & \vdots & \vdots & \vdots & \vdots & \vdots \\ 0 & 0 & \dots & 1 & 0 & 0 & 0 & \dots & 1 & 0 & \frac{-\pi f r_{i(j-1)}}{\beta} \\ 0 & 0 & \dots & 1 & 0 & 0 & 0 & \dots & 0 & 1 & \frac{-\pi f r_{ij}}{\beta} \\ 0 & 0 & \dots & 0 & 1 & 1 & 1 & \dots & 1 & 1 & 0 \end{bmatrix}_{(ij+1)\times(i+j+1)} \times \begin{bmatrix} lnS_1(f) \\ \vdots \\ lnS_j(f) \\ lnG_1(f) \\ \vdots \\ lnG_i(f) \\ \frac{1}{Q(f)} \end{bmatrix}_{(i+j+1)\times 1}$$

$$= \begin{bmatrix} lnA_{11}(f) + \gamma lnr_{11} \\ lnA_{12}(f) + \gamma lnr_{12} \\ \vdots \\ lnA_{i(j-1)}(f) + \gamma lnr_{i(j-1)} \\ lnA_{ij}(f) + \gamma lnr_{ij} \\ 0 \end{bmatrix}_{(ij+1)\times 1} \tag{2.10}$$

It can be seen from equation 2.10 that the data observed at one station from one event, the corresponding epicentral distance r_{ij} and spectral amplitude A_{ij} can be used to construct one row for matrices $\mathbf{G}$ and $\mathbf{d}$, respectively. The generalized inverse of equation 2.8 is

then solved using a singular-value decomposition procedure (SVD) (Menke, 1990) of $\mathbf{G}$ to give an estimation of the model parameters $\mathbf{m}$ by fixing f and using known variables A , r, and β for each source-receiver pair.

The matrix $\mathbf{G}$ can be written as a multiplication of three matrices:

$$\mathbf{G} = \mathbf{V}\mathbf{U}\Lambda^T \tag{2.11}$$

where $\mathbf{U}$ is a diagonal matrix containing singular values of the matrix $\mathbf{G}$ on its diagonal and has the same size as $\mathbf{G}$. Matrices $\mathbf{V}$ and Λ are unitary square matrices and the columns of each of them form a set of orthonormal vectors. So, the inverse of vector $\mathbf{G}$ for each frequency passband with a center frequency f can be calculated as follows:

$$\mathbf{G}_g^{-1} = \mathbf{V}\Lambda^{-1}\mathbf{U}^T \tag{2.12}$$

Then as stated above, using the SVD procedure the vector $\mathbf{m}$ can be written as

$$\mathbf{m} = \mathbf{G}_g^{-1}\mathbf{d}. \tag{2.13}$$

We simultaneously inverted for the source spectrum term for each event and site term for each station as well $Q^{-1}(f)$. The inversion is done independently for each of the eight frequency passbands with center frequencies f set at at 1.0, 1.3, 2.0, 3.0, 4.0, 6.0, 8.0, and 10.0 Hz. This gives a Q estimate at the center frequency f of each passband of interest.

To fit the Q estimates into a frequency-dependent function $Q(f)$, I modeled $Q(f)$ using the power law in equation 2 using a linear least-squares regression analysis based on the

elimination method as it was done with Tok earthquake data analysis.

Taking the natural logarithm of equation 2 and solving the equation $lnQ(f) = lnQ_0 + \eta ln(f)$ for lnQ_0 and η when the reference frequency f_0 is set equal to 1.0 Hz results in the frequency-dependent function $Q(f)$ representing the attenuation across Alaska.

RESULTS AND DISCUSSION

A spectral amplitude decay method has been implemented in this study to determine the frequency dependence of the seismic attenuation in Alaska using seismic records from one event (Tok earthquake) at first and then using numerous events spanning a period of four years (2014-2018). We first used this method to determine frequency-dependent attenuation in different azimuths in eastern Alaska using waveform recordings from the Tok earthquake. Then the same method was used to get frequency-dependent attenuation results using amplitude measurements of Lg waves from data recorded in Alaska in a four-year period (2014-2018). This method requires dense event and station coverage as what is currently in Alaska to yield good estimates. This method allowed us to obtain Lg Q estimates over Alaska and the frequency-dependent function $Q(f)$ representing the area.

Results

Results from the Tok, AK Earthquake

To study the attenuation in different directions of an earthquake, we selected four different azimuthal profiles and estimated $Q(f)$ function along each one of the selected profiles (see Figures 7 - 10). In addition, we analyzed the horizontal ground motions in these profiles to understand the effect of distance on attenuation and to look at any possible crustal structure variations and boundaries. Figures 12- 15 represent the horizontal ground motions for all four profiles from the Tok earthquake. In these figures, ground motions

are plotted against epicentral distance to look for any strong visible change in slope that may be related to a change in attenuation with distance beyond 200 km. The presence of the change in slope would indicate a transition boundary and crustal variation that may need further investigation for confirmation.

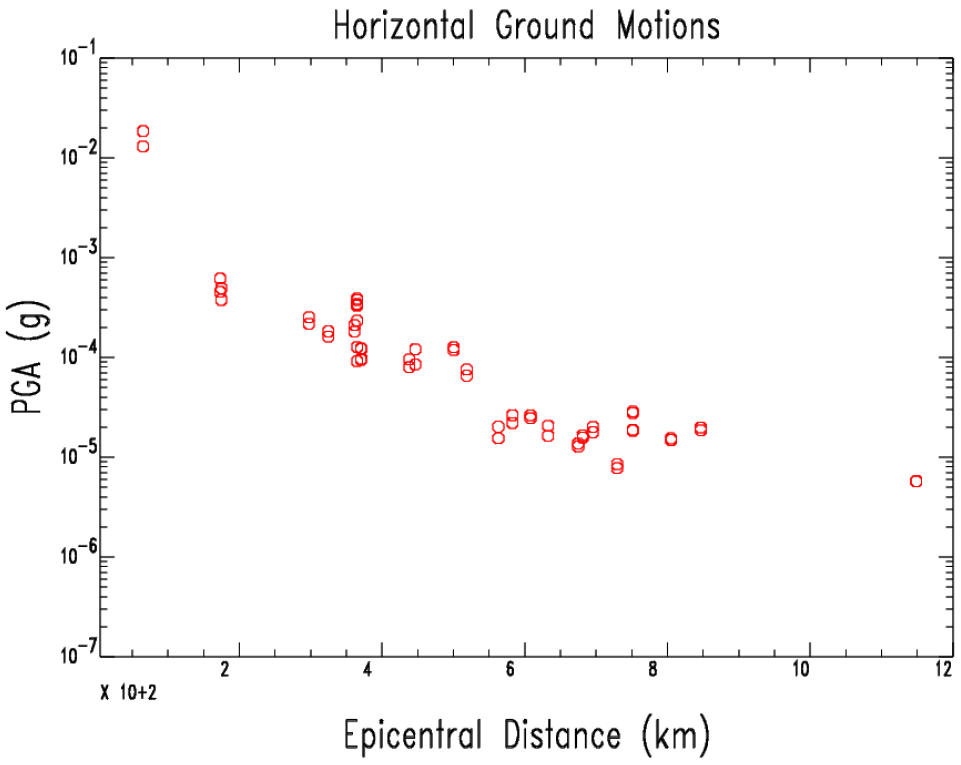

FIGURE 12: Tok earthquake: Southwestern profile

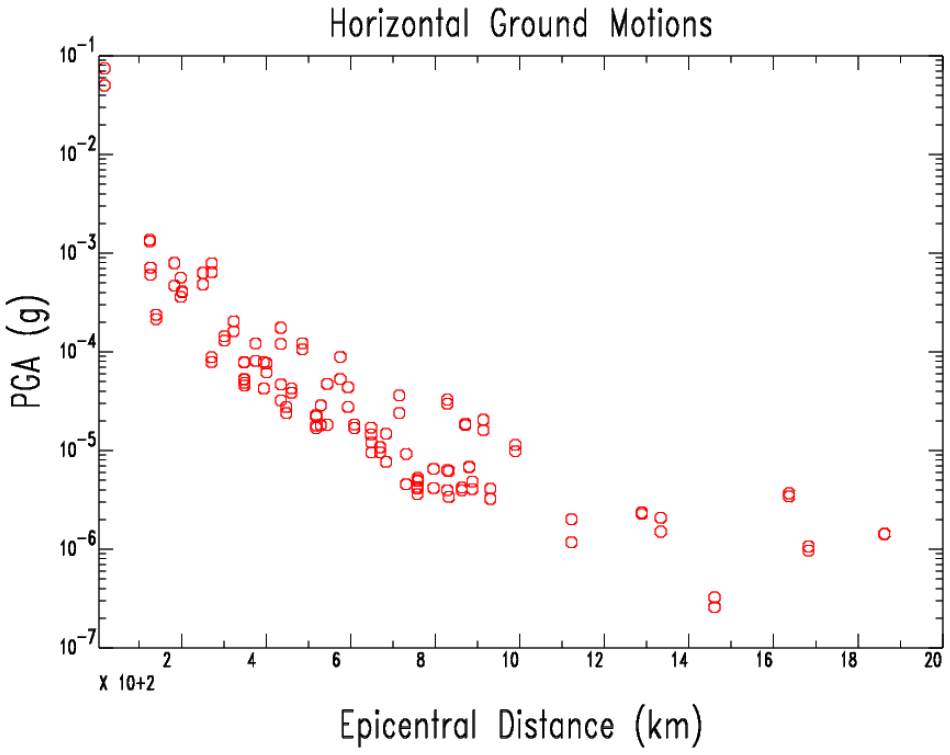

FIGURE 13: Tok earthquake: Northwestern profile

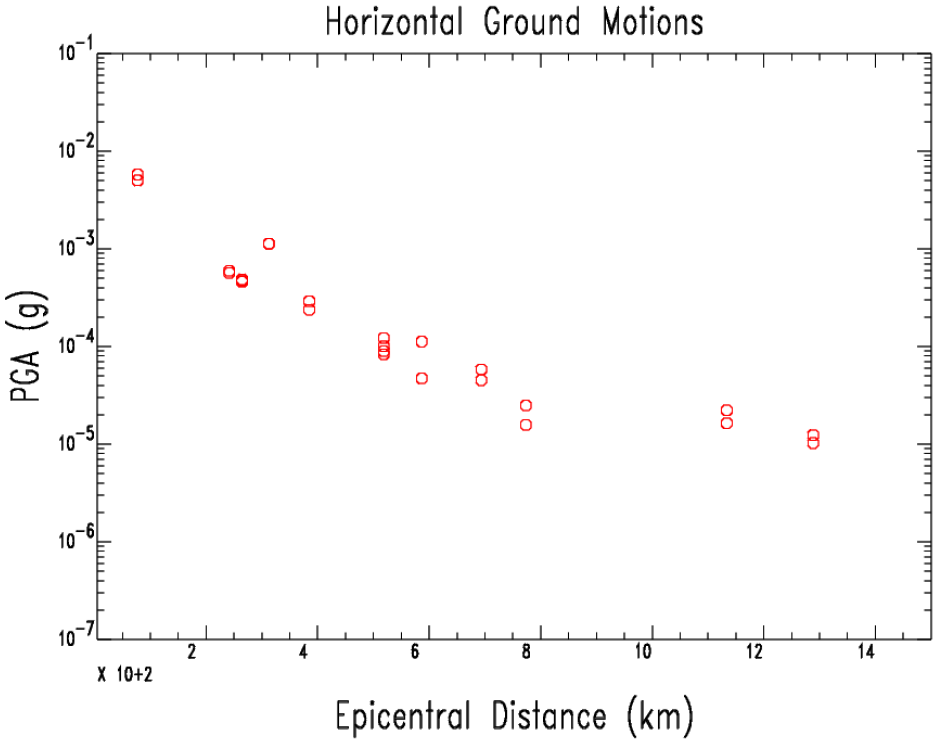

FIGURE 14: Tok earthquake: Northeastern profile

H

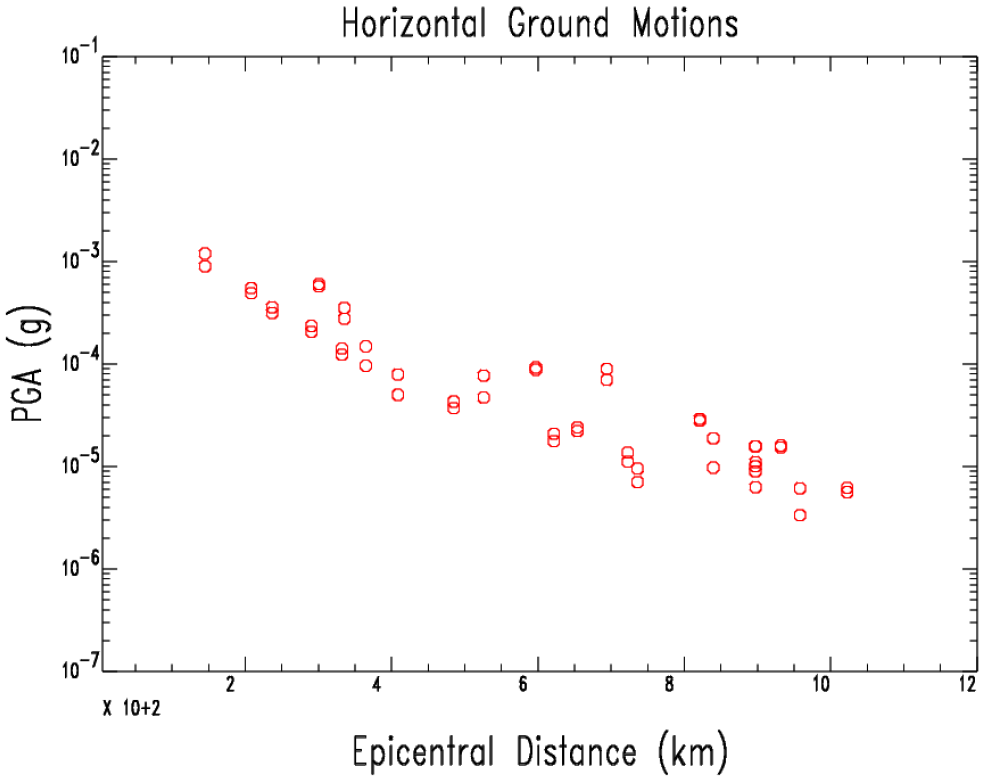

FIGURE 15: Tok earthquake: Southeastern profile

Notice in all figures a decay of the peak ground acceleration (PGA) with distance. However, the PGA decays at different rates and flattens and/or dissipates at different distances for all profiles. In the southwestern profile (Figure 12), peak ground acceleration flattens in the distance range of 550-850km and then dissipates at distances between 175 km and 300 km as well as at distances between 850 km and 1150 km from the epicenter. In the northwestern profile (Figure 13), the PGA flattens at distances between 700 km and 900 km from the epicenter and then it dissipates or gets scattered at distances beyond 900 km from the epicenter while in the northeastern profile (Figure 14), it dissipates at a distance between 750 km and 1125 km from the epicenter. Finally, in the southeastern profile (Figure 15), the PGA dissipates at a distance of 500 km from the epicenter and then flattens at a slow rate at distances beyond 600 km from the epicenter.

The PGA dissipation may be caused by lack of stations; however, the flattening at different distances likely represents seismic wave signals hitting a noise floor. In addition to the peak ground acceleration decay at different distances, we observe a PGA dissipation followed by a decrease in PGA at distances less than 200 km (distances near the source) which is likely related to strong geometrical spreading effects.

Using the Q estimates obtained from equation 2.5 for each of the ten center frequencies, we estimated $Q(f)$ along each one of the selected profiles by fitting all Q estimates at all frequencies in the equation 2.6 using the elimination method to slove for lnQ_0 and η. The result is a straight line in logarithmic scale with an equation of the form $Q(f)$ $=Q_0 f^{\eta}$ representing frequency-dependent Q of each profile. The figures below summarize the results.

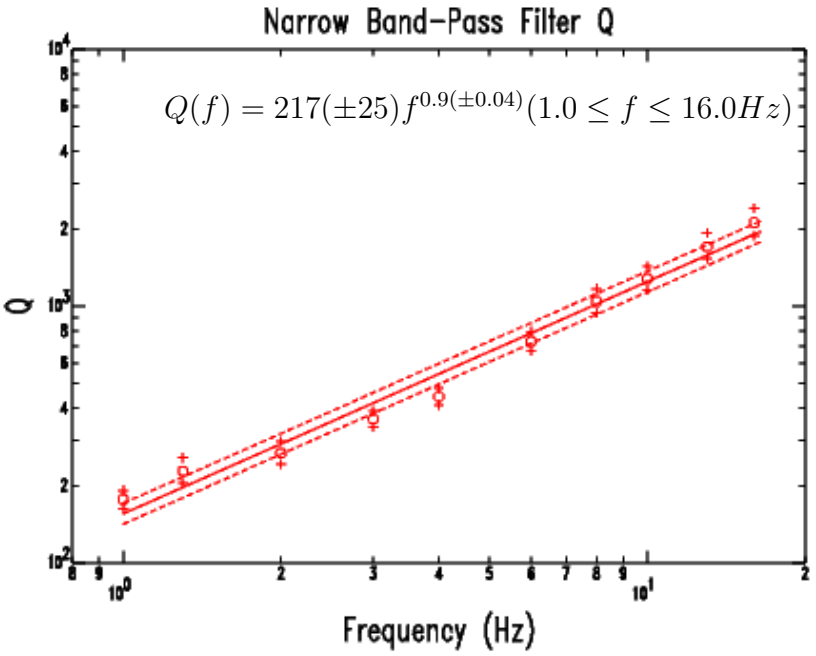

FIGURE 16: Tok earthquake: Southwestern profile.
Lg Q estimates in each profile as a function of frequency ($1.0 \leq f \leq 16Hz$). Solid line is the least square regression fit using Equation 2 and the dashed lines are 95 % confidence limits of the regression.

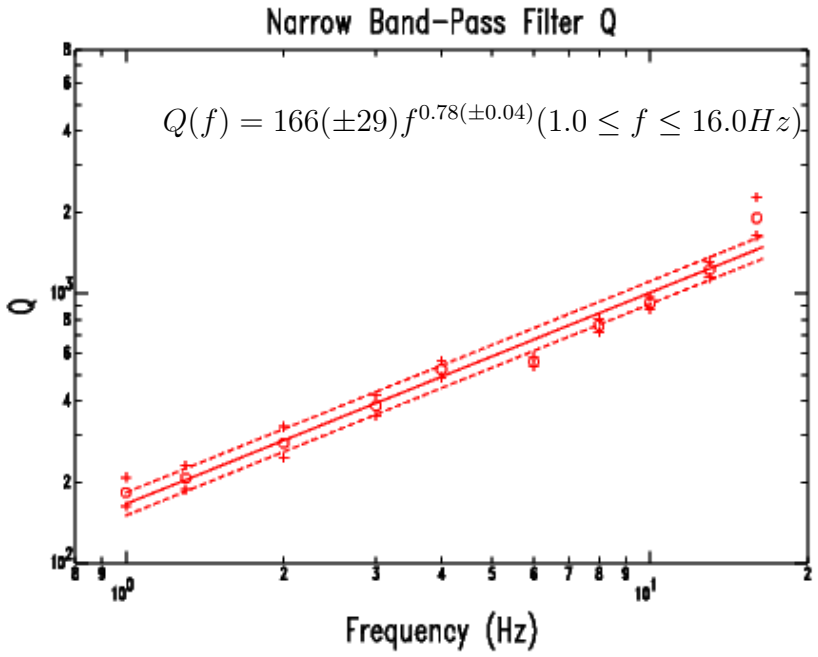

FIGURE 18: Tok earthquake: Northeastern profile. Symbols are the same as in Figure 16.

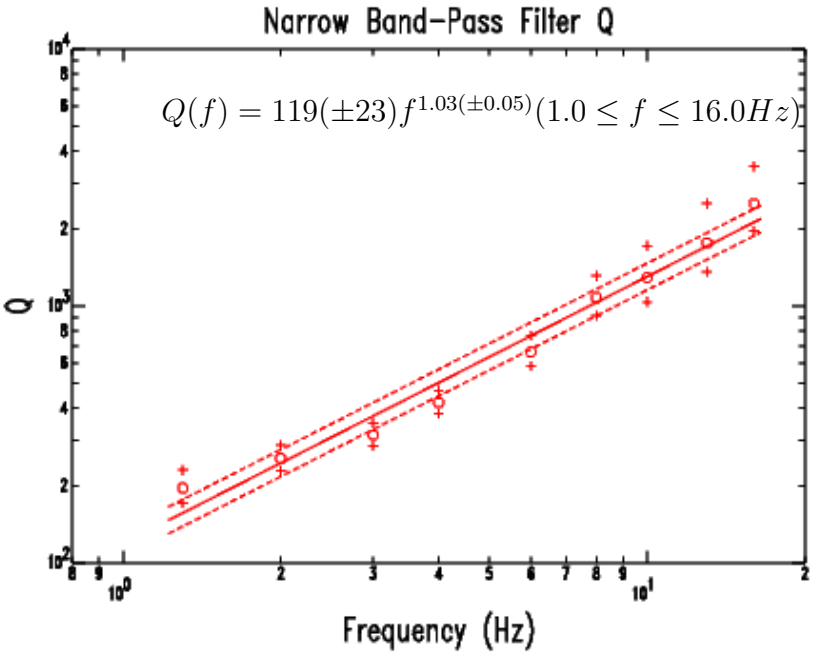

FIGURE 17: Tok earthquake: Northwestern profile. Symbols are the same as in Figure 16.

Looking at figures 16 - 19, we notice low Q_0 and high η values indicating a tectonically active region with high Lg attenuation associated with strong frequency dependence. The

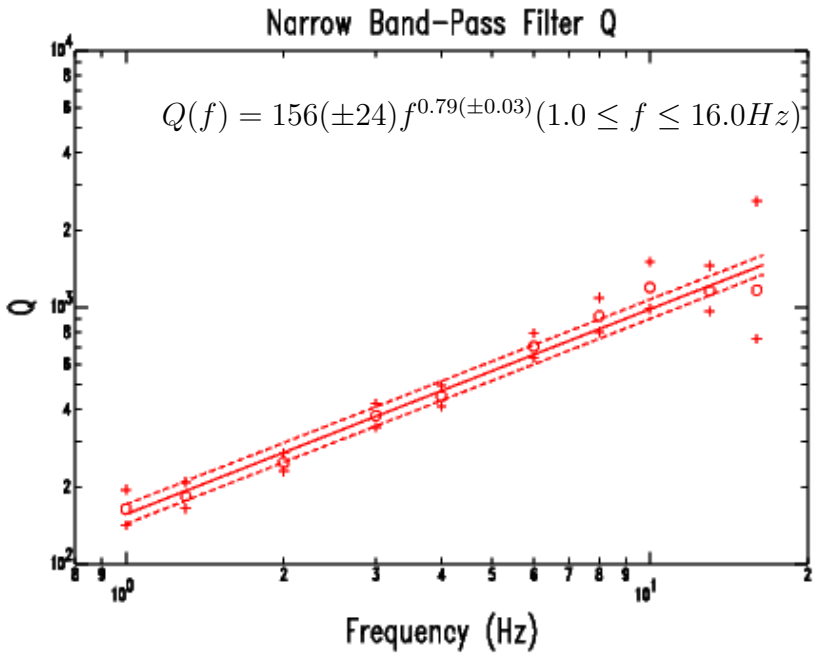

FIGURE 19: Tok earthquake: Southeastern profile. Symbols are the same as in Figure 16.

values differ from one profile to another which implies different degrees of heterogeneity in Alaska's crust. In addition, these four profiles show Q_0 values in the same range as the values obtained by Erickson et al. (2004) in other tectonically active regions like northern California, southern California, and the Rocky Mountain states. The high Lg attenuation in our study area may be a result of a combination of various geologic factors including subduction, volcanism, and faulting. All these factors may have an impact on attenuation by creating favorable conditions for high absorption of Lg wave. These favorable conditions include but are not limited to fractures, variations in the crust, and increase of crustal temperature.

Results from 2014-2018 events

Regional Lg Average Q

After looking at the preliminary results from the Tok earthquake, we calculated frequency-dependent Lg Q for the whole of Alaska using events from data collected in a 4-year period (2014 - 2018). More than 8000 Lg amplitude observations from 187 events recorded at current stations in Alaska (Figure 3) were used for the inversion. The data used were limited to the distance range of 100 to 1000 km.

Using equations 2.7-2.13, we inverted data at all center frequencies using a least squares regression. However, due to the constraint of the center frequencies to be below half of Nyquist frequency, we obtained Lg amplitude decay as a function of epicentral distance (Figure 21) and Q_{Lg} estimates (Table 3) for only eight center frequencies (1.0, 1.3, 2.0, 3.0, 4.0, 6.0, 8.0, and 10.0 Hz).

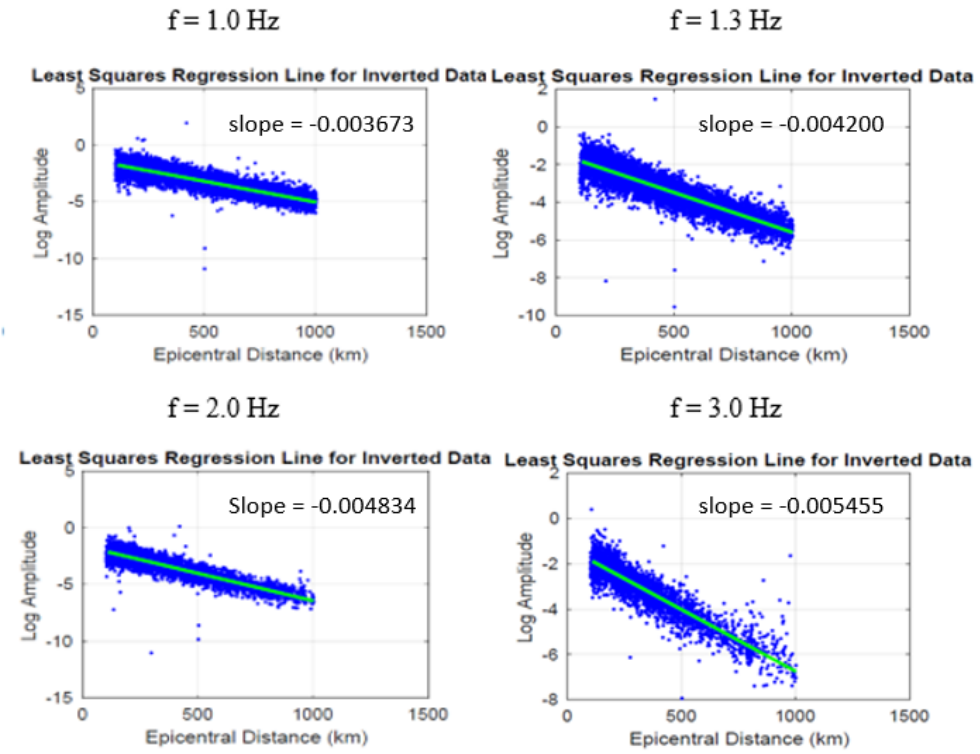

FIGURE 20: Lg spectral amplitude decay as a function of distance at 1.0, 1.3, 2.0, and 3.0 Hz.

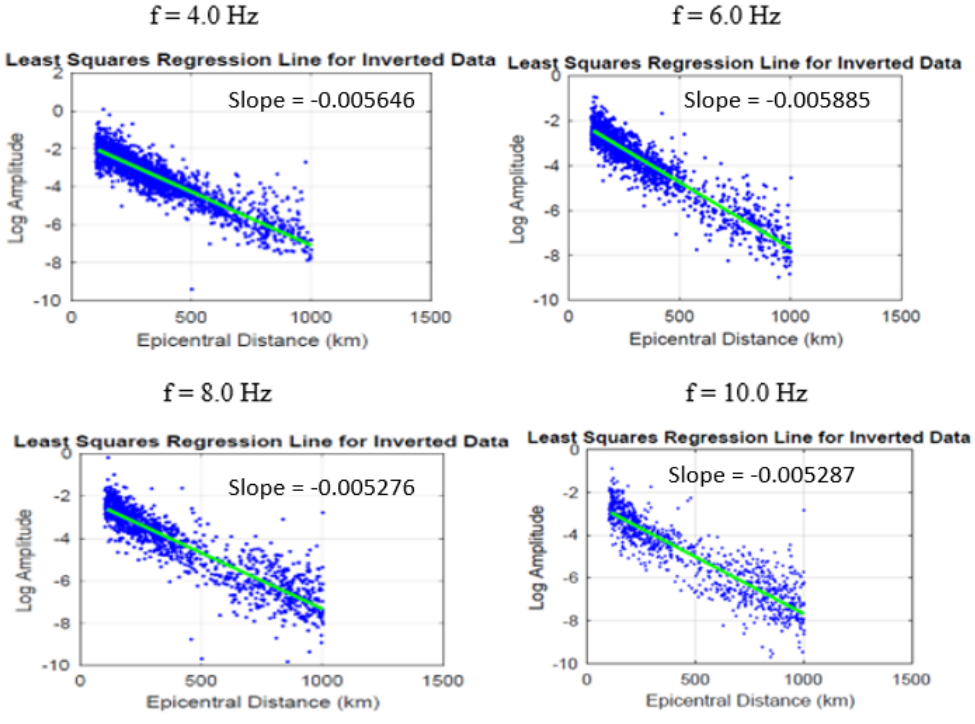

FIGURE 21: Lg spectral amplitude decay as a function of distance at 4.0, 6.0, 8.0, and 10.0 Hz.

Figure 20 and Figure 21 summarize Lg spectral amplitude decay for Alaska at each frequency of interest. Looking at values of the slopes in Figure 21, there is a trend of a decrease in the steepness of the slope with increase of frequency. However, starting at f = 8.0 Hz the trend changes and the steepness of the slope increases dramatically and then starts the decreasing trend as the frequency reaches 10.0 Hz. This change in trend may be due to poor resolution at higher frequencies and contamination at high frequencies. In addition, at lower frequencies (f = 1.0, 1.3, 2.0, 3.0, and 4.0 Hz) the inverted data are concentrated around the mean fit for the whole range of distance of interest (100 - 1000 km) while at higher frequencies (f = 6.0, 8.0, and 10.0 Hz) the inverted data scatter increases as the frequency increases at distances beyond 500 km. This may be caused by high-frequency Sn coda contaminating the Lg window at larger distances.

With Q_{Lg} values listed in Table 2 for each center frequency f, we determined the best-fit line in the range of passbands (1.0 to 10.0 Hz) as an estimate of frequency-dependent Q for the region. A linear least-squares regression based on the elimination method as it was done by Cramer (2018) is used to fit Q estimates into equation 2.6. The result is a straight line in logarithmic scale (see Figure 22) with the equation $Q(f) = 217(\pm 28)f^{0.84(\pm 0.04)}$ $(1.0 \leq f \leq 10.0Hz)$ representing Alaska's regional frequency-dependent Lg attenuation.

TABLE 2: Estimates of Lg Attenuation at each frequency in Alaska.
$Q_{max} = Q + Q_{std}$ and $Q_{min} = Q$ - Q_{std} where Q_{std} is the error estimate for the inversion and is different from the confidence intervals for the regression shown in figure 22.

Frequency (Hz)	Q	Q_{max}	Q_{min}
1.0	244.390	244.951	243.829
1.3	277.796	278.571	277.022
2.0	371.384	372.811	369.957
3.0	493.674	496.706	490.643
4.0	635.927	641.117	630.737
6.0	915.073	931.053	899.093
8.0	1361.004	1383.07	1338.938
10.0	1697.893	1731.883913	1663.902

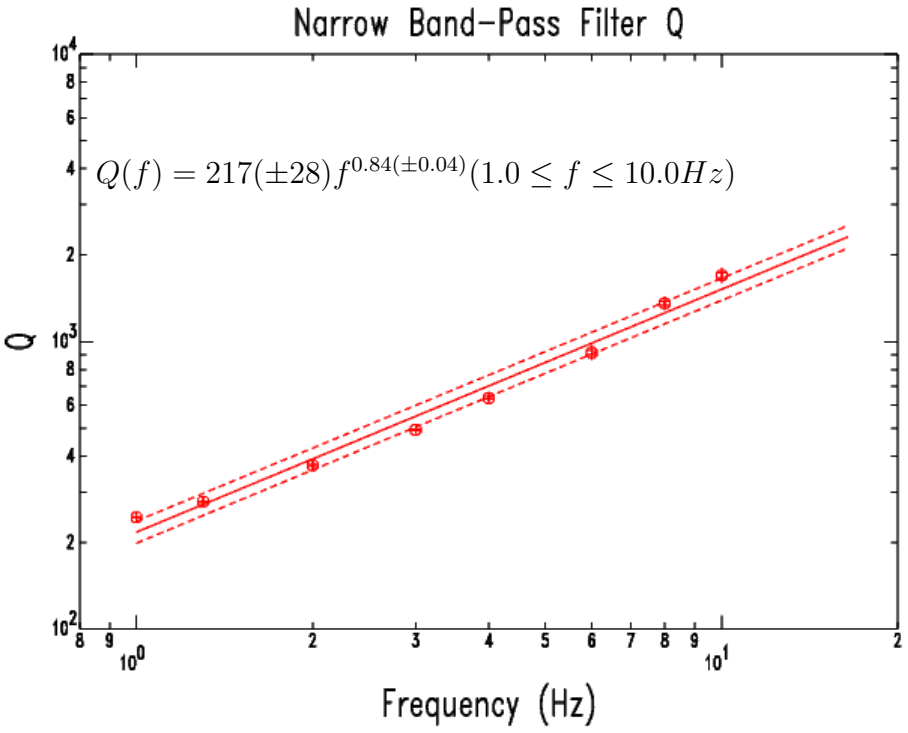

FIGURE 22: Regional Lg Q estimates as a function of frequency. Solid line is the least square regression fit using Equation 2 and the dashed lines are 95 % confidence limits of the regression.

Spatial Variations

In order to study the spatial variations of Lg Q throughout Alaska, we divided Alaska in four rectangular subregions: North, South-central, Southeast and Southwest (Figure 23) and then calculated the seismic attenuation in these regions. We set up coordinates defining each region of interest before the inversion so that the Q inversion method only uses events and stations located in the pre-set coordinates for each region. The figures 24 - 27 show the attenuation as a function of frequency and the $Q(f)$ function for these regions.

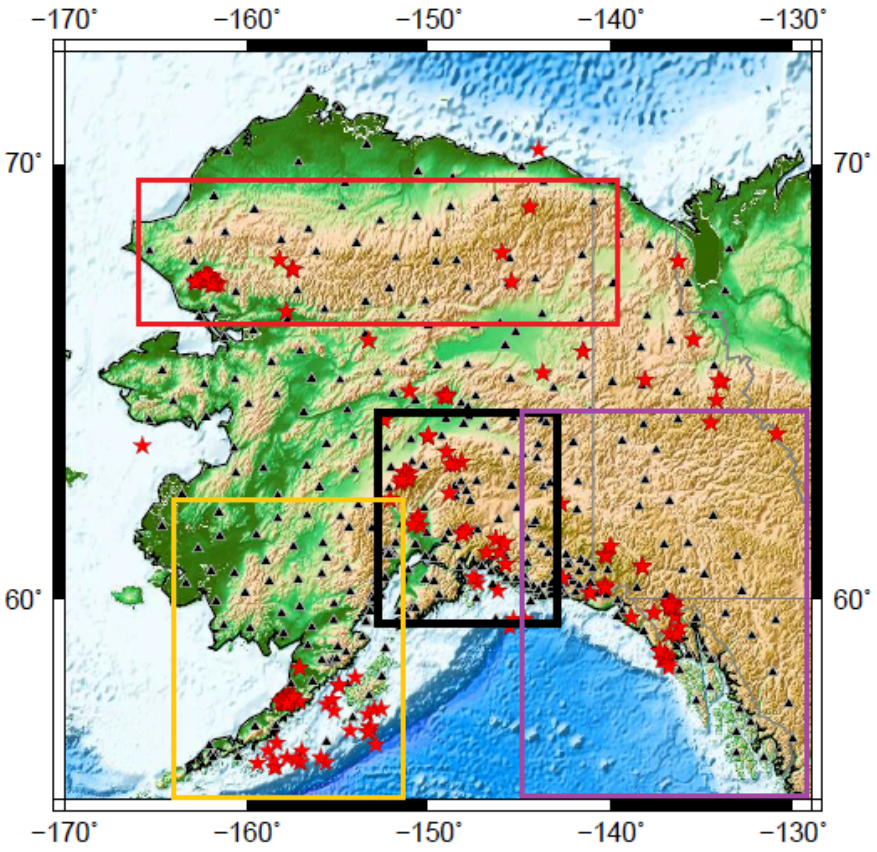

FIGURE 23: Alaska divided in four sub-regions represented by colored rectangles. Gold: Southwest, Black: South-central Alaska, Purple: Southeast, and Red: North. The figure was generated using GMT. An open source software available at: https://gmt.soest.hawaii.edu.

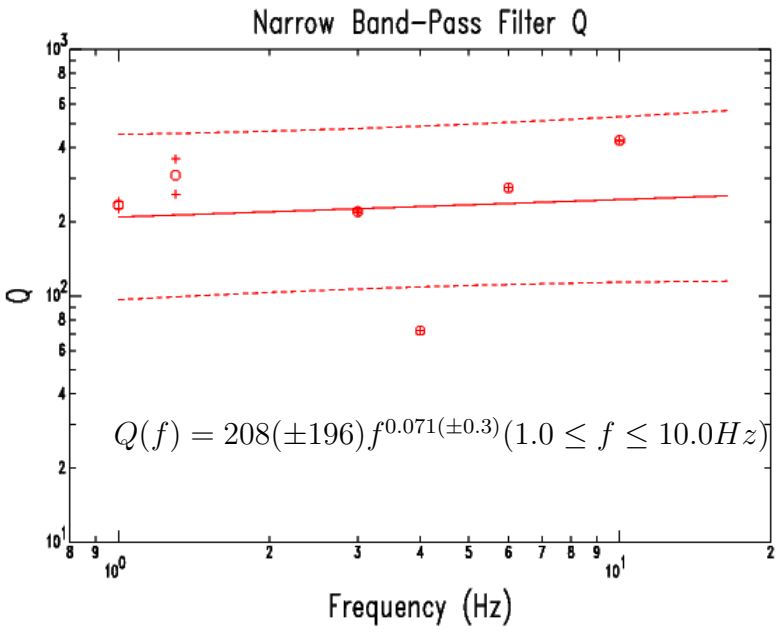

FIGURE 24: Northern profile (66°N to 69°N and -138°W to -166°W). Solid line is the least square regression fit using Equation 2 and the dashed lines are 95 % confidence limits of the regression.

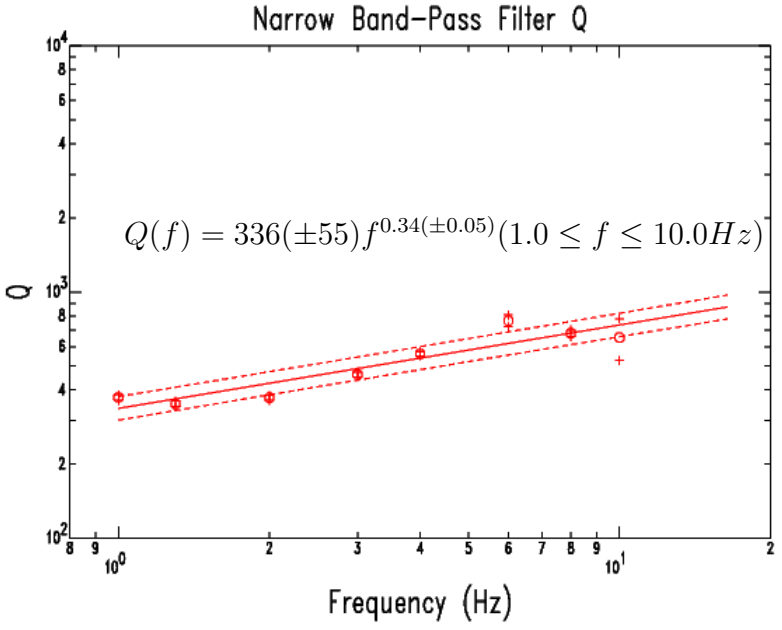

FIGURE 25: South-central profile (59°N to 64°N and -143°W to -152°W). Symbols are the same as in Figure 24.

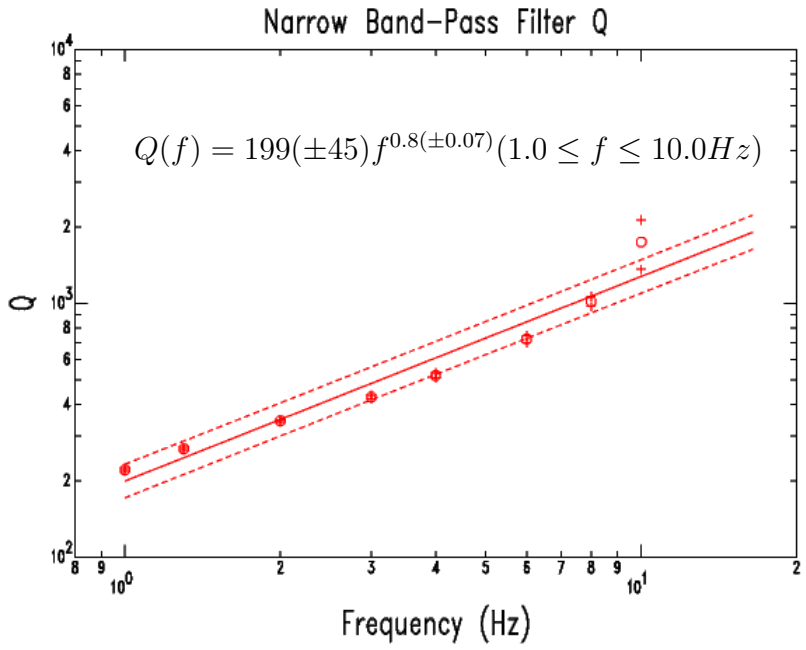

FIGURE 26: Southeastern profile (54°N to 64°N and -130°W to -145°W). Symbols are the same as in Figure 24.

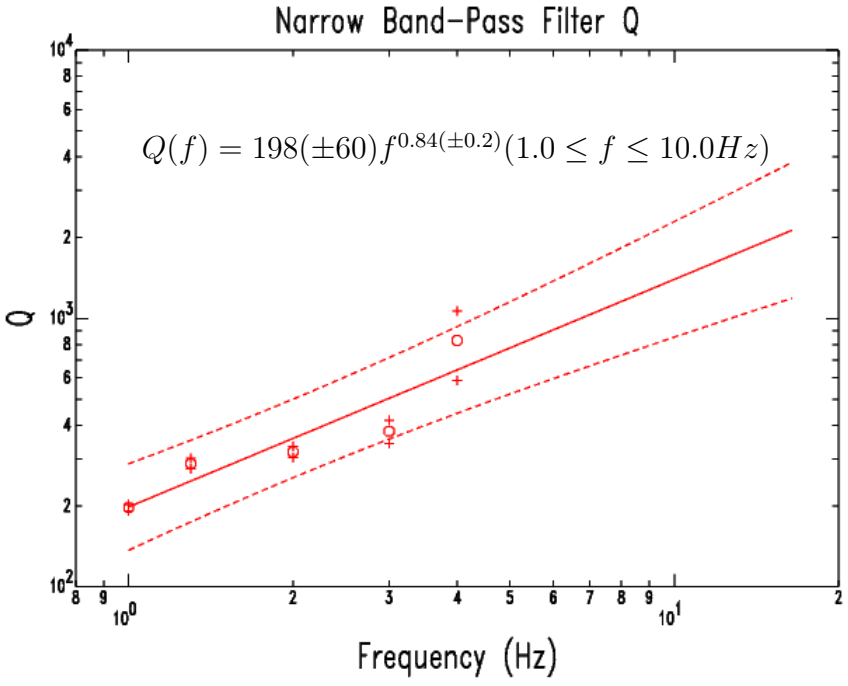

FIGURE 27: Southwestern profile (54°N to 62°N and -151°W to -164°W).Symbols are the same as in Figure 24.

Looking at figures 24 - 27, we see areas of high attenuation (low Q_0 value) associated with strong frequency dependence (high η value) in the Southeast and the Southwest (Figure 26 and Figure 27, respectively.). On the other hand, we see area of lower attenuation than others (high Q_0 value) associated with weak frequency dependence (low η value) in the South-central region (Figure 25). Then we have Northern region characterized by high attenuation (low Q_0 value associated with a very high error) with almost no frequency dependence (η=0.071 with error of 0.3). The results shown in the figures above are related to seismicity, tectonics, geology, and ray-path coverage in each one of the considered subregions.

The south-central area is a very active region. It is an area with high seismicity due to the proximity to the subduction zone and numerous tectonically active mountain ranges such as the Alaska Range, Wrangell Mountains, and Aleutian Range. Considering the presence of all these features in addition to crustal deformation which extends over 500 km inland in south-central Alaska (Haynie and Jadamec, 2017), we expected a high Lg wave attenuating area; but the obtained results indicate a moderate attenuation in this area. With a Q_0 of 336 and η of 0.34, south-central Alaska would be considered a seismically stable region (low attenuation with weak frequency dependence), but not as stable as the central and northeast United States (Erickson et al., 2004) or eastern Canada (Mousavi et al., 2014). This contradiction, however, can be explained by the presence of a flat slab segment of the Pacific plate beneath the south-central Alaskan lithosphere (Haynie and Jadamec, 2017).

This flat slab region is characterized by high seismicity and a thin lithosphere above it (less than 25 km) [as cited in Haynie and Jadamec (2017)]. In addition to a thin lithosphere,

there is a presence of young mountain ranges in the flat slab region. This area's younger age and thin lithosphere can both contribute to a strong attenuation in the area. However, there is a cold mantle wedge which causes a lack of volcanism above the slab (Stachnik et al., 2004). Thus, lack of volcanism and low temperatures contribute to a low Lg attenuation in south-central Alaska. These competing factors in south-central Alaska combined with other factors like variations and deformations in the crustal structure are the reason the south-central Alaska area has a moderate Lg attenuation as observed in this study, but not as low as stable continental regions like CEUS and eastern Canada.

The Northern region's Q_0 value has a high standard deviation and the error estimate in η is greater than its actual value. Looking at Figure 2, the Northern region can be designated as a seismically inactive region. Usually in regions with low seismic activity (stable regions), high Q_o and low η values are expected. However, the equation representing Northern region (Figure 24) indicates a low Q_o value associated with a very high standard deviation (poorly resolved). This contradiction may be a result of lack of data in the area. Figure 4 indicates that the Northern region was not covered by recording stations before the deployment of TA stations in Alaska and Western Canada. Therefore there were not enough data in this region to be used in calculations causing the poor results.

When considering Southeastern and Southwestern subregions, we see a trend of Q_0 values lower than 200. These low Q_0 values make sense because the tectonics in these two regions are driven by the movement of the Pacific plate creating favorable conditions for high absorption of Lg waves. Both regions have an abundance of shallow earthquakes due to transform motion of the Pacific plate passing the North American plate in the Southeast and subduction of the Pacific plate under the American plate in the Southwest. The

transform motion causes fractures and faults while the subducting motion deforms the crust towards the inland generating variations in crustal structure (Veenstra et al., 2006) and volcanism in the Southwest direction. Therefore, the highly fractured crust, the faults and the variations in crustal structure absorb high-frequency seismic waves, Lg waves included, causing high Lg wave attenuation (low Q_0). In addition, both regions have mountain ranges with active and inactive volcanoes which would contribute heavily to Lg wave absorption and cause strong attenuation.

The Q_0 and η values of the Southeast area agree with the results obtained analyzing data from the Tok earthquake indicating a seismically active region with high attenuation (low Q_0) and strong frequency dependence (high η value) in this direction. In contrast to southeastern region, the Q_0 value in southwestern region has a high standard deviation as it can be seen on the mean fit and the linear equation that best fits the Q estimates in this region (see Figure 27). This might be caused by surface wave contamination at higher frequencies, events located offshore skewing the results, unknown instrument response or a combination of all three.

Error Analysis

The frequency-dependence function, $Q(f)$, obtained directly from Lg waves is subjected to different sources of errors. Thus, for each frequency passband, a delete-j jackknife resampling technique was used to calculate errors related to the inversion (Erickson et al., 2004). The delete-j jackknife technique used in this study consists of throwing out a randomly selected 10% of the data from the total number of observations to create a new

jackknife dataset and then inverting each jackknife dataset to determine Q values using the least squares regression method.

Using all the Q values obtained from inverting the new jackknife datasets, we were able to estimate the mean and standard deviation. For our error bound, we dropped 2.5% for lower bound and 2.5% for higher bound of the Q values calculated from the jackknife dataset for accuracy. Figure 28 shows the results obtained from 50 different inversions of randomly selected Jackknife datasets at 3.0 Hz.

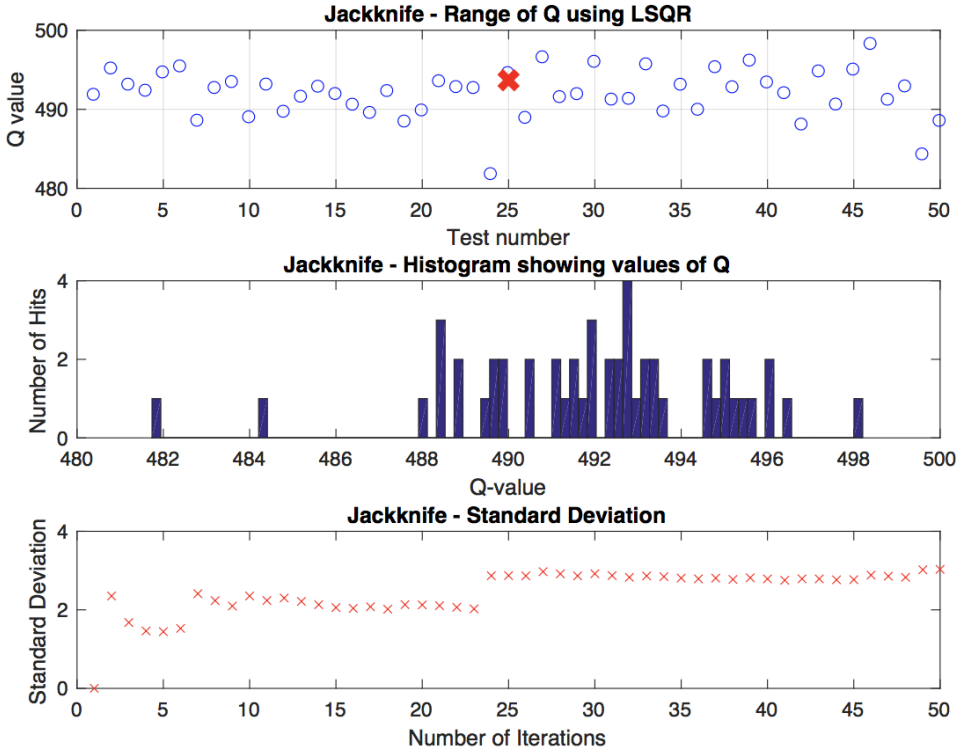

FIGURE 28: Jackknife technique results plots from this study at 3.0 Hz.

Looking at Figure 28, the top plot shows the Q value of each of the 50 randomly selected jackknife datasets at each inversion performed. The red X represents the actual Q value calculated from the complete dataset at 3.0 Hz. The plot in the middle shows a histogram of the results obtained from 50 different inversions of 50 randomly selected Jackknife

datasets at 3.0 Hz. The bottom plot shows the jackknife standard deviation for each new jackknife dataset at 3.0 Hz.

As an example, the average jackknife Q value at 3.0 Hz is 491.95 while the complete dataset Q is 493.67 and the standard deviation is 3.03. Looking at figure 28, the histogram looks like a normal distribution with a high peak at about 493 corresponding to the Q value calculated from the complete dataset and the average jackknife Q value at this frequency.

Discussion

Taking advantage of current dense coverage of Alaska that was made possible by the USArray TA project, we estimated the frequency-dependent attenuation for Alaska and its spatial variations using the spectral amplitude decay of Lg waves. The regional frequency-dependent attenuation of Alaska is given by the equation $Q(f) = 217(\pm 28)f^{0.84(\pm 0.04)}$ $(1.0 \leq f \leq 10.0Hz)$ and the graph showing the attenuation as a function of frequency is plotted in figure 22. The Q_0 value of 217 indicates a tectonically active region. This is supported by high seismicity observed in figure 2. The η value of 0.84 implies that the Lg wave attenuation in Alaska is highly frequency dependent. Alaska's strong Lg wave attenuation observed in this study is likely a result of contributions from the subduction process, Alaska's geology, and volcanism present in Alaska and its vicinity.

The subduction mechanism causes heterogeneity and deformations in the crust. The Alaska crustal deformation extends over 500 km inland (Plafker and Berg, 1994). With high crustal deformation, a strong Lg wave attenuation in the overlying plate should

be expected because it causes the variations in crustal thickness in the upper plate. In addition to the subduction process, Alaska consists of numerous crustal fractures and active faults like the Denali fault, Kobuk fault, and Castle Mountain faults resulting from the subduction process. Lg amplitudes may attenuate significantly due to scattering along these fractures and faults. Furthermore, volcanic activities from numerous mountain ranges in Alaska may cause high temperature and heat the Alaskan crust to cause partial melting in areas like southwest causing high seismic attenuation. Therefore, the subduction process and several other geologic activities like volcanism and faulting that are likely happening beneath Alaska including but not limited to the ones stated above likely contribute to Alaska's high crustal Lg attenuation observed in this study.

Comparing our results to other studies that have been conducted in different regions, we see that our results are in agreement with those obtained in south central Alaska (McNamara, 2000). In addition, our results are in the same range as the results in the Gulf Coast (Cramer, 2018), the Caribbean (Hosseini et al., 2015), and the Basin and Range Province (Erickson et al., 2004). However, the Q_0 values in California and the Pacific Northwest (Erickson et al., 2004) are lower and the Q_0 values in central and eastern United States (Erickson et al., 2004), and eastern Canada (Mousavi et al., 2014) are higher than Q_0 and η values from this study. Below is a comparison between this study's results and other attenuation studies that have been done in other seismically active regions.

TABLE 3: Lg Q and η values from selected studies including this study.

Region	Q_0	η	**Reference**
Northern California	152	0.72	Erickson et al. (2004)
South California	105	0.67	”
Pacific Northwest	152	0.76	”
Rocky mountain states	166	0.61	”
Basin and Range Province	200	0.56	”
Alaska	217	0.84	This study
South-central Alaska	220	0.66	McNamara (2000)
Caribbean	235	0.65	Hosseini et al. (2015)
Gulf Coast region	259	0.715	Cramer (2018)
Eastern Canada	615	0.35	Mousavi et al. (2014)
Central United States	640	0.34	Erickson et al. (2004)
Northeast United states	650	0.36	”

Looking at the Table 3, our Q_0 value is close to that determined by McNamara (2000) in the south-central Alaska for his results between 0.75 and 12.0 Hz with $Q(f) = 220(\pm 30) f^{0.66(\pm 0.09)}$. In contrast, southern and northern California, the Pacific Northwest, and the mountain states all have high Lg attenuation associated (low Q) with strong frequency dependence(high η). These very low Q_0 values are most likely related to the geology and seismicity in these regions. They are tectonically active regions. In California, the geological structures include numerous active faults like the San Andreas fault that are found throughout California, active volcanism at several locations like Lassen Volcanic Park, and geothermal

activity near Clear Lake. In the Pacific Northwest, the high Lg attenuation may be the result of the presence of the Cascade volcanoes and partial melting beneath the Columbia plateau (Phillips and Stead, 2008). The Yellowstone hotspot being located in the center of the mountain states region, likely influences the attenuation in the area (Erickson et al., 2004).

On the other hand, the Q_0 values in central and eastern United States (CEUS) and eastern Canada indicate stable continental regions with lower attenuation than Alaska. These high Q_0 values result from age, thermal status, geology and tectonics in both regions. In southeast Canada the low Lg attenuation is related to low average heat flow, lack of fluid, and thick and cold lithosphere (Zhao and Mousavi, 2018). In addition, it may be related to Canadian Shield's old age since the Q_{Lg} increases with the age of the region since its last major tectonic event [as cited in Zhao and Mousavi (2018)].

The CEUS region consists of numerous inactive faults and low heat flow in most of the region except in the northern portion of the Gulf Coastal Plain (GCP) and along the border of South Dakota and Nebraska. In addition, it is mostly covered by a thin and dry sediment except in areas along GCP, the Mississippi embayment, the southern Oklahoma Aulacogen and Reelfoot Rift where the sediment is thick, porous and contains fluids (Gallegos et al., 2014). Apart from those anomalous areas with high attenuation as reported by Gallegos et al. (2014), the old age, the thermal status, the geology and the lack of recent tectonic activity in most of the CEUS contribute to a low Lg attenuation as shown in table **??** [Gallegos et al. (2014) and Erickson et al. (2004)].

The method used in this study is very convenient because not only can we solve for regional Lg Q we can also solve for the source and station terms, S and G using the SVD

technique. By solving for both source term and site response, we can get more crustal properties like wave velocity, density of the near surface formations at the recording stations, and amplification effects from the site response and also we can estimate earthquake magnitude accurately using the source term if necessary. However, the drawback with the SVD inversion method applied during the course of this study is the use of several assumptions.

One assumption is the use of Lg group velocity of 3.5 km/s. This group velocity is assumed based on the fact that Lg is not dispersive and Lg wave energy arrives in the group velocity window 3.6 to 2.9 km/ sec [as cited in Erickson et al. (2004)].

Another assumption is the constant geometric spreading γ. Selecting a proper geometrical spreading exponent γ is a challenge because of the trade-off between geometrical spreading and seismic attenuation when solving for both simultaneously and the choice of γ can affect the final results. Underestimating γ leads to an underestimation of Q_0 and an overestimation of η and vice versa (McNamara et al., 1996). Usually γ varies between 0.5 and 0.8. In this study we use γ of 0.5 because it is the commonly used value in Lg wave attenuation studies. However, γ can be computed using the model proposed by Atkinson and Mereu (1992) in which the value of γ changes as a function of epicentral distance r_{ij} [as cited in (Hosseini et al., 2015)]. This γ value computation may improve the attenuation results.

CONCLUSION

Q variations depend on tectonic structure of the region. Several studies that have been done on attenuation in different regions show that Lg waves attenuate more rapidly in tectonically active regions than stable continental regions. Therefore, the stable continent regions have high Q_0 and low η values while tectonically active regions have low Q_0 and high η values. The linear equation $Q(f) = 217(\pm 28)f^{0.84(\pm 0.04)}$ best represents Lg-wave frequency-dependent attenuation in Alaska on a log-log plot. The Q_0 and η values indicate a tectonically active region with high Lg attenuation (low Q_0) that is strongly frequency dependent (high η). The subduction process and several other geologic activities like volcanism, high heat flow, crustal heterogeneity and deformation that are likely happening in different parts of the Alaskan lithosphere influence high crustal attenuation. Direct comparison of this study's results with results from other regions (Table **??**) shows that Alaska's Q_0 value is in the range of seismically active regions and falls between tectonically active areas like California and stable continental regions like the CEUS and the northeastern United States.

As with previous studies done in Alaska, we encountered the problem of lack of data during analyses in regions like northern and western Alaska which did not have stations before the arrival of USArray. The installation of stations in a 3-year period created the problem of lack of enough data in north and western Alaska because stations in these regions were installed in the last phase of installation. Because all the stations are now in place, a more detailed and more accurate study can be done. This future study would be able to address questions like crustal variations, location of Q boundaries, if there are any, and attenuation based regionalization of Alaska.

Bibliography

Aki, K. (1969). Analysis of the seismic coda of local earthquakes as scattered waves. *Journal of Geophysical Research*, 74(2):615–631.

Aki, K. and Chouet, B. (1975). Origin of coda waves: Source, attenuation, and scattering effects. *Journal of Geophysical Research*, 80(23):3322–3342.

Atkinson, G. M. and Mereu, R. (1992). The shape of ground motion attenuation curves in Southeastern Canada. *Bulletin of the Seismological Society of America*, 82(B3):2014–2031.

Bath, M. (1954). The elastic waves Lg and Rg along Euroasiatic paths. *Arkiv Geofysik Stockholm*, 2(2):295–342.

Benz, H. M., Frankel, A., and Moore, D. M. (1997). Regional Lg Attenuation for the Continental United States. *Bulletin of the Seismological Society of America*, 87(3):606–619.

Bouchon, M. (1982). The complete synthesis of seismic crustal phases at regional distances. *Journal of Geophysical Research: Solid Earth*, 87(B3):1735–1741.

Brocher, T. M., Fuis, G. S., Fisher, M. A., Plafker, G., Moses, M. J., Taber, J. J., and Christensen, N. I. (1994). Mapping the megathrust beneath the north Gulf of Alaska using wide-angle seismic data. *Journal of Geophysical Research*, 99(B6):11,663–11,685.

Brogan, G. E., Cluff, L. S., Korringa, M. K., and b. Slemmons, D. (1975). Active faults of Alaska. *Tectonophysics*, 29(1–4):73–85.

Chiu, K. and Snyder, D. B. (2014). Regional seismic wave propagation (lg sn phases) in the amerasia basin and high arctic. *Polar Science*, 9(2015):130–145.

Cormier, F. V. (2011). Seismic, Viscoelastic Attenuation. In Gupta, H. K., editor, *Encyclopedia of Solid Earth Geophysics*, chapter 33, pages 1279–1289. Springer, Dordrecht, The Netherlands.

Cramer, C. H. (2018). Gulf Coast Q and Boundaries from USArray Data. *Bulletin of the Seismological Society of America*, 108(1):437–449.

Erickson, D., Mcnamara, D. E., and Benz, H. M. (2004). Frequency-Dependent Lg Q within the ContinentalUnited States. *Bulletin of the Seismological Society of America*, 94(5):1630–1643.

Fan, G.-W. and Lay, T. (2003). Strong Lg Attenuation in the Tibetan Plateau. *Bulletin of the Seismological Society of America*, 93(5):2264–2272.

Furumura, T., Hong, T., and Kennett, B. L. (2014). Lg wave propagation in the area around Japan: observations and simulations. *Progress in Earth and Planetary Science*, pages 1–10.

Gallegos, A., Ni, J., Ranasinghe, N., and Sandvol, E. (2014). Lg attenuation in the central and eastern United States as revealed by the Earthscope Transportable Array. *Earth and Planetary Science Letters*, 402:187–196.

Goldstein, P., Dodge, D., Firpo, M., and Minner, L. (2003). SAC2000: Signal processing and analysis tools for seismologists and engineers. In Lee, W., Kanamori, H., and Jennings, P., editors, *The IASPEI International Handbook of Earthquake and Engineering Seismology*. Academic Press, London, UK.

Hansen, R., McNamara, D., and Ark, E. V. (1998). Lg Propagation characteristics in Continental Alaska. *EOS.Trans.AGU*, 79.

Haynie, K. L. and Jadamec, M. A. (2017). Tectonic drivers of the Wrangell block: Insights on fore-arc sliver processes from 3-D geodynamic models of Alaska. Tectonics(36):781–784.

Herrmann, R. B. and Nuttli, O. W. (1982). Magnitude: the relation of M_L to m_{bLg}. *Bulletin of the Seismological Society of America*, (72):389–397.

Hosseini, M., Pezeshk, S., Haji-Soltani, A., and Chapman, M. (2015). Investigation of Attenuation of the Lg-wave Amplitude in the Caribbean Region. *Bulletin of the Seismological Society of America*, 105(2):734–744.

Kennett, B. L. (1986). Lg waves andStructural boundaries. *Bulletin of the Seismological Society of America*, 76(4):1133–1141.

Kim, W.-Y. and Richards, P. G. (2007). North Korean nuclear test: seismic discrimination at low yields. *Bulletin of the Seismological Society of America*, (14):157–161.

Knopoff, L., Schwab, F., and Kausel, E. (1973). Interpretation of Lg. *Geophysical Journal International*, 33(4):389–404.

Main, I. G., Naylor, M., Greenbough, J., Touati, S., Bell, A. F., and McCloskey, J. (2011). Model selection and uncertainty in earthquake hazard analysis. In Faber, M., Koehler, J., and Nishijima, K., editors, *Applications of Statistics and Probability in Civil Engineering*, pages 735–743. Taylor Francis Group, London.

McNamara, D. E. (2000). Frequency Dependent Lg Attenuation in South-central Alaska. *Geophysical Research Letters*, 27(23):3949–3952.

McNamara, D. E., Owens, T. J., and Walter, W. R. (1996). Propagation Characteristics of Lg across the Tibetan Plateau. *Bulletin of the Seismological Society of America*, 86(2):457–469.

Menke, W. (1990). *Introduction to Seismology*, volume 45. Academic Press Inc., San Diego, CA, third edition.

Mitchell, B. J. and Hwang, H. J. (1987). Effect of low Q sediments and crustal Q on Lg attenuation in the United States. *Bulletin of the Seismological Society of America*, 77(4):1197–1210.

Mousavi, S. M., Cramer, C. H., and Langston, C. A. (2014). Average Q_{Lg}, Q_{Sn}, and observation of Lg blockage in the Continental Margin of Nova Scotia. *Journal of Geophysical Research: Solid Earth*, 119(10):7722–7744.

Nuttli, O. W. (1973). Seismic wave attenuation and magnitude relations for eastern North America. *Journal of Geophysical Research: Solid Earth*, 106(78):876–885.

Ottemöller, L., Shapiro, N. M., Singh, S. K., and Pacheco, J. F. (2002). Lateral variation of Lg wave propagation in southern Mexico. *Journal of Geophysical Research*, 107(B1):ESE 3–1–ESE 3–13.

Phillips, W. S. and Stead, R. J. (2008). Attenuation of Lg in the western US using the USArray. *Geophysical Research Letters*, 35(7):1–5.

Plafker, G. and Berg, H. C. (1994). *Overview of the geology and tectonic of Alaska*, volume G-1, chapter 33, pages 989–1021. The Geological Society of America, Boulder, CO.

Redfield, T. and Fitzgerald, P. (1993). Denali Fault System of southern Alaska: An interior strike-slip structure responding to dextral and sinistral shear coupling. *American Geophysical Union*, 12(5):1195–1208.

Ruppert, N. A. and Hansen, R. A. (2010). Temporal and Spatial Variations of Local Magnitudes in Alaska and Aleutians and Comparison with Body-Wave and Moment Magnitudes. *Bulletin of the Seismological Society of America*, 100(3):1174–1183.

Shearer, P. M. (2009). *Introduction to Seismology*. Cambridge University Press, Cambridge, UK, second edition.

Stachnik, J. C., Abers, G. A., and Christensen, D. (2004). Seismic attenuation and mantle wedge temperatures in the alaska subduction zone. *Journal of Geophysical Research: Solid Earth*, 109(B10):1–16.

Steensma, G. and Biswas, N. (1988). Frequency dependent characteristics of coda wave quality factor in central and south-central Alaska. *PAGEOPH*, (128):295–307.

Stein, S. and Wysession, M. (2003). *An introduction to Seismology, Earthquakes, and Earth Structure*. Number 23. Blackwell Publishing Ltd, Malden, MA.

Veenstra, E., Christensen, D. H., Abers, G. A., and Ferris, A. (2006). Crustal thickness variation in south-central Alaska. *Geology*, 34(9):781–784.

Xie, J. (2002). Lg Q in the Eastern Tibetan Plateau. *Bulletin of the Seismological Society of America*, 92(2):871–876.

Zhao, L.-F. and Mousavi, S. M. (2018). Lateral Variations of Crustal Lg Attenuation in Eastern North America. *Scientific Reports*, 8(7285):217–234.